Marine Structures 97 (2024) 103654

Contents lists available at ScienceDirect

Marine Structures

journal homepage: www.elsevier.com/locate/marstruc

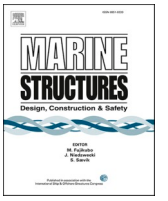

Ultimate strength of welded aluminium stiffened panels under combined biaxial and lateral loads: A numerical investigation

Xintong Wang *, Zhaolong Yu, Jørgen Amdahl

Centre for Autonomous Marine Operations and Systems (AMOS), Department of Marine Technology, Norwegian University of Science and Technology, Trondheim, 7050, Norway

ARTICLE INFO

Keywords:
Aluminium
Welding
Ultimate strength
Combined load
Lateral pressure
HAZ

ABSTRACT

The number and size of aluminium non-monohull ships have been steadily increasing over time. This raises growing concerns regarding their structural strength, especially considering the adverse effects of the heat-affected-zone (HAZ) on welding connections in aluminium structures. This paper investigates the ultimate strength of welded aluminium stiffened panels under combined biaxial compressive loads and lateral pressure through the application of numerical simulations. Altogether 360 cases are simulated with varied panel lengths, welding patterns and load combinations. The results are presented and discussed with respect to force end-shortening curves, failure modes and ultimate strength. Influences of the combined loads and HAZ effects are summarized. The numerical results are compared to two commonly used design methods in the marine industry, the International Association of Classification Societies (IACS) rule and the Panel Ultimate Limit States (PULS) approach. Their applicability to welded aluminium stiffened panels is discussed, and modifications are suggested with respect to the transverse loads, lateral pressure, and HAZ effects.

1. Introduction

With the superior properties of good formability, high strength-to-weight ratio, high recyclability and corrosion resistance, aluminium has been widely used in the aviation, automotive, and civil industries. For the design of marine structures, aluminium provides an environmental-friendly lightweight solution. For example, the superstructures, living quarters, gangways and helicopter decks of ships and offshore platforms have been manufactured in aluminium for decades. In addition, aluminium is often preferred for hulls of small sized vessels such as working boats and ferries. With reduced structural weight and carbon emissions, both the number and size of aluminium vessels increase constantly [1] and will continuously increase in the future.

Aluminium ships are often designed as catamarans or trimarans due to the hydrodynamical and functional benefits. Such special hull shapes have higher probabilities of encountering transverse bending and wave slamming than monohulls, in which case longitudinal, transverse, and lateral loads can appear simultaneously in certain areas such as cross-decks shown in Fig. 1. Thus, it is necessary to investigate the structural strength under combined loads, notably the elementary stiffened panels of marine structures.

Different approaches exist in the literature for structural strength analysis. Experiments often provide valuable information. Combined loads were shown to strongly influence the failure modes [2–5] for steel stiffened panels. Buckling experiments of aluminium stiffened panels, which have different material properties and are more vulnerable to the overall buckling mode [6,7], are

* Corresponding author.
E-mail address: xintong.wang@ntnu.no (X. Wang).

https://doi.org/10.1016/j.marstruc.2024.103654
Received 22 February 2024; Received in revised form 11 April 2024; Accepted 5 June 2024
Available online 12 June 2024

still lacking to some extent. Most studies reported in the literature have used the nonlinear finite element method (NLFEM) to investigate the resistance of aluminium stiffened panels under combined loads [8–11]. Accordingly, empirical formulations were derived based on a number of simulated cases [11]. The simulations, however, cover mainly cases under combined uniaxial compression and lateral pressure. Studies considering biaxial compression are limited [12]. Since the interaction effects between load components are substantial for stiffened panels, numerical investigations with combined biaxial compression and lateral load are needed. To ensure simulation accuracy under different load combinations, the model extents, material properties, boundary conditions, welding effects and mesh techniques need to be carefully considered. Detailed discussion related to numerical modelling can be found in the benchmark studies by International Ship and Offshore Structures Congress (ISSC) for both steel and aluminium stiffened panels [13,14].

Another crucial factor that influences the strength of aluminium marine structures is the welding effects. The unavoidable welding connections produce geometrical imperfections. The most used imperfection field for steel marine structures is the 'Hungry Horse' (HH) model [15]. For extruded aluminium stiffened panels, the HH model was found to be applicable by Wang and Amdahl [16]. By summarizing experimental measurements with a number of welded aluminium stiffened panels, Paik et al. [17] developed a set of deterministic imperfections. Georgiadis et al. [18,19] developed a stochastic geometric imperfection field, which intended to overcome improper combinations of deterministic imperfection fields and amplitudes. After welding, tensile residual stresses retain near the welds and compressive residual stresses in the remaining area of the cross-section. The magnitude of residual stresses varies in different studies, and its influence was found to depend on the plate and column slenderness in previous research [20,21]. In addition, the heat input generates a heat-affected-zone (HAZ) along the weld for aluminium alloys, where the material yield strength reduces. The extent of material softening depends on the aluminium alloy types and welding techniques, and the reduction of material yield stresses in HAZ can vary from 33 % to 90 % in different studies [22–25]. Extensive studies have been conducted to understand the welding effects on the strength of aluminium structures [13,16,20,26–32], but with limited work considering combined loading conditions.

To understand better the fundamental behaviour of aluminium stiffened panels and to verify and improve existing design methods, this paper investigates numerically their ultimate strength subjected to combined biaxial compression and lateral pressure, considering the welding effects.

The paper is structured as follows: Design methods, especially the International Association of Classification Societies (IACS) rule and the Panel Ultimate Limit States (PULS) approach, are introduced in Section 2. The numerical model assumptions and setups are then discussed in Section 3. Force end-shortening curves, failure modes and ultimate strength from the numerical simulations are presented in Section 4, and the influence of combined loading and welding effects are also discussed. The numerical results and the design method predictions are compared. Potential improvements of the design methods for welded aluminium stiffened panels are discussed in Section 5. The conclusions are summarized in Section 6.

2. Design methods

In the preliminary structural design stage, the ultimate load carrying capacity of a structure is of major concern. Simple formulations based on analytical and semi-analytical methods are developed and used for this purpose.

To establish and develop minimum design requirements, the International Association of Classification Societies (IACS) adopted the Common Structural Rules for Bulk Carriers and Oil Tankers (CSR) in 2013 and updated it in 2018. In the rule the ultimate strength of stiffened panels is predicted by defining failure categories as global panel buckling, local plate buckling/yielding and local stiffener buckling/yielding. It is worth noting that in the old rule, the one-dimensional beam theory, which applied an equivalent lateral pressure for all in-plane load combinations, was found to be inaccurate and subsequently replaced with the elastic buckling theory of orthotropic plates in the updated version [33,34]. Accordingly, the class guideline DNV-CG-0128 Buckling from the Det Norske Veritas (DNV) followed the update in 2021 edition [35].

Besides, the DNV-RP-C201 Buckling Strength of Plated Structures [36] provides recommended practice for the design of unstiffened plates and orthogonal stiffened panels. Buckling of unstiffened plate is resolved with the effective width method. Its capacity formulations (buckling curves) depend on loading conditions. The failure of stiffened panels is treated as the buckling of a beam-column with an equivalent cross-section, buckling length and loading conditions. The recommendations covers biaxial compression, shear stresses and lateral pressure [37].

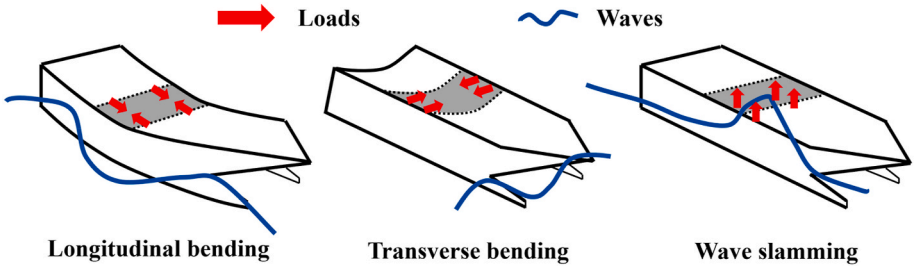

Fig. 1. Potential loads of large aluminium catamarans.

A different semi-analytical method was developed by Byklum and Amdahl [38–40] to assess the buckling strength of unstiffened and stiffened plates using large deflection plate theory and energy principles. It combines local and global stresses with an incremental procedure in a computer program PULS (Panel Ultimate Limit States) by DNV [41].

In addition, global buckling of stiffened panels can be numerically solved using large deflection orthotropic plate theory [42–44], where the stiffened panel is represented by an orthotropic plate with equivalent elastic modulus, and flexural and torsional rigidities. The stress distribution due to load interaction is analysed for the orthotropic plate, and the ultimate strength is predicted based on first material yielding. The method was further extended by Benson et al. [7] to account for the overall panel buckling mode for aluminium stiffened panels.

Despite the fact that most design methods are mainly developed for steel structures, they are capable of predicting the strength of aluminium structures in many cases. A study by Wang et al. [45] showed that the DNV-CG-0128 rule, which is same as the IACS rule, could be applied to aluminium stiffened panels with butt welding also when longitudinal loads predominate. PULS can consider aluminium structures that are fabricated in different ways by introducing material reduction factors at different critical check points [41]. The IACS rule and the PULS approach are further described with respect to governing ultimate limit states and the evaluation methodologies. More detailed formulations can be found in the related design rule [34] and the PULS user manual [41].

2.1. IACS common structural rules (2018 version)

Three ultimate state limits are defined in the IACS rule as shown in Fig. 2.

(1) Elastic stiffened panel limit (Global buckling of stiffened panels)
(2) Plate buckling limit (Local plate buckling and yielding)
(3) Stiffener ultimate limit (Local stiffener buckling and yielding)

The first limit represents elastic buckling of the stiffened panel. Failure occurs when the elastic buckling stress is reached. The second limit checks elastic buckling of plates between stiffeners. Elastic buckling of a panel is however, not considered to be critical, as a substantial reserve capacity can be expected in the post buckling stage due to constrained edges. Failure is considered to occur when the plate material starts yielding. The third limit covers possible buckling and yielding of stiffeners with attached plate flanges. The failure modes of local stiffened panels can be complicated in reality, but in the IACS rule different modes are considered by one common failure criterion that checks material yielding at the top and bottom fibers of the stiffener at the midspan.

The elastic stiffened panel limit is based on interaction between the various load components. Orthotropic plate theory with smeared stiffeners is assumed. In the case with only biaxial loads, the stress multiplier factor $\gamma_{GEB,bi}$, which represents the inverse of the usage factor, is given as:

$$\gamma_{GEB,bi} = \frac{\pi^2}{L_{B1}^2 L_{B2}^2} \bullet \frac{\left[D_{11} L_{B2}^4 + 2(D_{12} + D_{33})\right] n^2 L_{B1}^2 L_{B2}^2 + n^4 D_{22} L_{B1}^4}{L_{B2}^2 N_x + n^2 L_{B1}^2 K_{tran} N_y} \tag{1}$$

where N_x and N_y are the applied force in the longitudinal and transverse directions, respectively; L_{B1} is the stiffener span; L_{B2} is the panel width; n is the number of half waves in the transverse direction; K_{tran} is a coefficient taken as 0.9; D_{ij} are bending stiffness coefficients of the stiffened panel.

The plate buckling limit subjected to combined loading is based on an interaction formula. Neglecting the shear stress term and the safety factor, it is a von Mises type equation given as:

$$\left(\frac{\gamma_c \sigma_x}{\sigma_{cx}}\right)^{e_0} - B\left(\frac{\gamma_c \sigma_x}{\sigma_{cx}}\right)^{\frac{e_0}{2}} \left(\frac{\gamma_c \sigma_y}{\sigma_{cy}}\right)^{\frac{e_0}{2}} + \left(\frac{\gamma_c \sigma_y}{\sigma_{cy}}\right)^{e_0} = 1 \tag{2}$$

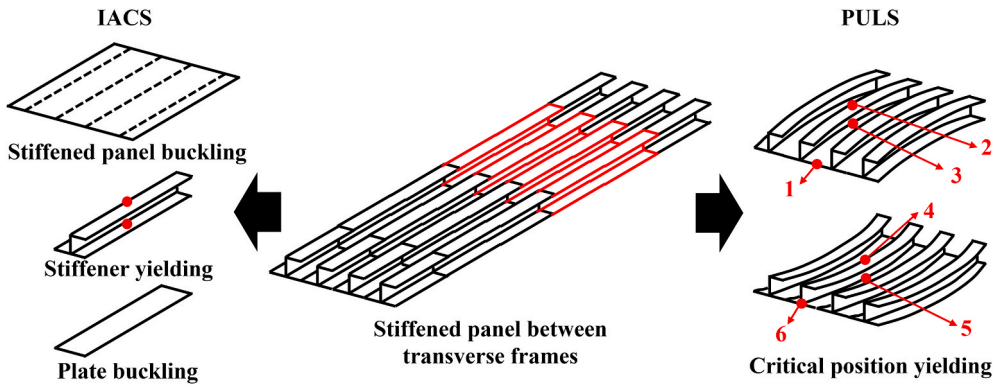

Fig. 2. Schematic illustration of failure categories.

where γ_c is the stress multiplier factor; σ_x and σ_y is the applied normal stress; σ_{cx} and σ_{cy} is the ultimate buckling stress; B and e_0 are coefficients depending on the plate slenderness and aspect ratio. The limit also encompasses plate buckling under uniaxial compressions, although the equations for this case are not provided here.

For the ultimate limit of the stiffeners, a stiffener with its attached plate is assumed, and the plate's effective width is determined accordingly. Neglecting the safety factor, the yielding check at the stiffener midspan is given as:

$$\frac{\gamma_c\sigma_a + \sigma_b + \sigma_w}{R_{EH}} = 1 \tag{3}$$

where σ_a is the effective axial stress; σ_b is the bending stress; σ_w is the stress due to torsional deformation; R_{EH} is the specified minimum yield stress.

The IACS rule is developed for steel marine structures so there is no preference related to the welding effects except for the influence on initial imperfections.

2.2. PULS approach

In the PULS approach, the deflections of a stiffened panel are represented by a series of trigonometric functions. The combinations of biaxial, lateral and shear loads are included in the response formulations using large deflection plate theory and energy principles. The incremental equilibrium equations are solved numerically. Global buckling of the panel is taken as an equivalent plate with general anisotropic stiffnesses from the local analysis of the stiffeners and plates.

The PULS approach has six ultimate limits to check based on the first yield criterion as follows.

(1) Plate criterion along the plate edges
(2) Stiffener tension criterion
(3) Plate compression criterion
(4) Stiffener compression criterion
(5) Plate tension criterion
(6) Stiffener bending criterion at support

Material yielding is evaluated both at midspan and closer to the ends. A schematic illustration of the control positions is given in Fig. 2. The ultimate strength of aluminium structures can be assessed by specifying the fabrication method and the extent of material softening at the corresponding locations.

3. Numerical model

The NLFEM software Abaqus was adopted to evaluate the ultimate strength of aluminium stiffened panels. This section provides an overview of numerical modelling details and settings. A total of 360 cases were simulated considering different panel lengths, welding patterns, loading conditions, and load levels.

3.1. Geometries and boundary conditions

The cross-deck of a high-speed catamaran ferry was chosen to model a multi-span stiffened panel, as shown in Fig. 3-a. The vessel has a length between perpendiculars of 54 m, a moulded breadth of 16.5 m and a draught of 2.24 m. The fully loaded displacement is 580 tons. The panel model includes two complete- and two half spans, and contains six stiffeners in the width direction as suggested by

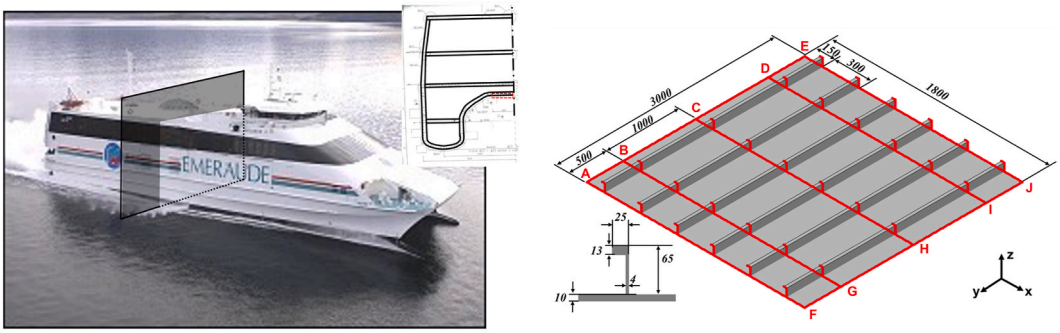

(a) Aluminium high speed catamaran ferry [46] and the investigated position

(b) Geometries of the stiffened panel

Fig. 3. Referred vessel [46] and geometry model of numerical simulations.

the class guidance DNV-CG-0128 Buckling [35]. The geometrical model allows the occurrence of interframe buckling in both the asymmetric mode (in/out) and the symmetric mode (in/in). The panel geometries are given in Fig. 3-b. The distance between transverse frames, l, is 1000 mm. The plate width between stiffeners, s, is 300 mm. The plate thickness, t, is 10 mm. The L-shaped stiffener has a web height, web thickness, flange width and flange thickness of 65 mm, 4 mm, 25 mm and 13 mm, respectively. The panel length varied from 400 mm to 1000 mm in 200 mm increments to investigate its influence.

The stiffened panels in the model are supported by robust transverse frames, fixing both vertical translation and longitudinal rotation along the edges. The detailed assignments of boundary conditions are given in Table 1.

Different loading conditions are considered. Uniaxial compression simulations were first conducted in displacement control. The loading velocity was 1 mm per second to mimic quasi-static conditions. In biaxial loading cases, a pre-stress was assumed in orthogonal direction, with a value of 25 %, 50 %, 75 % and 95 % of the uniaxial ultimate strength. Lateral pressure was applied on the plate side (external side). The pressure levels were taken as 0.1 MPa and 0.2 MPa, which represent a static water pressure of 10 m and 20 m, respectively. The lateral pressure values are chosen based on calculations with the Rule for Classification of High Speed and light Craft by DNV [47]. With the referred vessel size, the design slamming pressure on flat cross structures is 0.059-, 0.119-, 0.179- and 0.238-MPa for an acceleration of one to four times the gravity, respectively. The assumed values are representative in critical slamming scenarios.

Biaxial loading condition was achieved by displacement-controlled compression in a main loading direction and constant stresses along the boundary edges in the orthogonal direction as shown in Fig. 4. For the boundaries that were stress controlled, the edges were kept straight by imposing 'Kinematic Coupling Constraints' and free to move upon loading. The mid-point of the edge is chosen as the reference point of the 'Kinematic Coupling Constraints' as shown in the figure. Two loading scenarios, 'longi-controlled' and '*trans*-controlled', were defined depending on the main loading direction.

For combined loading conditions, the loading sequence matters and influences the ultimate strength [48]. The loading path curves in Fig. 5 shows the loading process in this work. The solid lines represent the longi-controlled cases with different transverse stress levels, while the dashed lines represent the *trans*-controlled cases with different longitudinal stress levels. The markers show the capacity drop points. The following loading path was adopted: The constant stress was first applied to the design level (red-shaded curve). Simultaneously, the constant lateral pressure was assigned. Then the displacement in the main loading direction was increased until the structure collapse with a capacity drop (blue-shaded curve).

It is noted that the loading path during the constant stress assignment is proportional. During this stage the displacement-controlled ends are fixed, which results in reaction forces due to the Poisson effects. The designed loading strategy has been used for hull plate and stiffened plate under combined loads [49–51] and the difference is found to be small compared to a proportional loading method.

3.2. Materials and welding effects

The Ramberg-Osgood relationship was used to model the AA6082-T6 aluminium alloys. The relationship between the stress and strain is expressed as [52]:

$$\varepsilon = \frac{\sigma}{E} + \alpha\frac{\sigma}{E}\left(\frac{\sigma}{\sigma_y}\right)^{n-1} \tag{4}$$

where E is the Young's modulus, ε is the strain, σ is the stress, α is the yield offset, σ_y is the yield stress, and n is the hardening exponent for the plastic term.

The parameters were calibrated to the experiments by Aalberg et al. [53], in which the material was fabricated by Hydro Aluminium Maritime using normal fabrication procedures [54]. One-sided full-penetration metal inert gas (MIG) butt welding was used to assemble the panels in their experiments. Three material properties were assumed for the plate, the stiffener, and the softened material in the HAZ, respectively. The stress-strain curves are shown in Fig. 6 and the parameters are given in Table 2.

The welding effects were introduced according to the work by Wang et al. [20], which showed good consistency with the 21

Table 1
Boundary conditions.

Edges	Displacement			Rotation		
	x	y	z	x	y	z
			Longitudinal controlled			
A-E	Free + Rigid	Free	Fixed	Fixed	Fixed	Fixed
E-J	Free	Displacement	Fixed	Fixed	Fixed	Fixed
A-F	Free	Fixed	Fixed	Fixed	Fixed	Fixed
F-J	Fixed	Free	Fixed	Fixed	Fixed	Fixed
B-G & C–H & D-I	Free	Free	Fixed	Free	Fixed	Free
			Transverse controlled			
A-E	Displacement	Free	Fixed	Fixed	Fixed	Fixed
E-J	Free	Free + Rigid	Fixed	Fixed	Fixed	Fixed
A-F	Fixed	Fixed	Fixed	Fixed	Fixed	Fixed
F-J	Fixed	Free	Fixed	Fixed	Fixed	Fixed
B-G & C–H & D-I	Free	Free	Fixed	Free	Fixed	Free

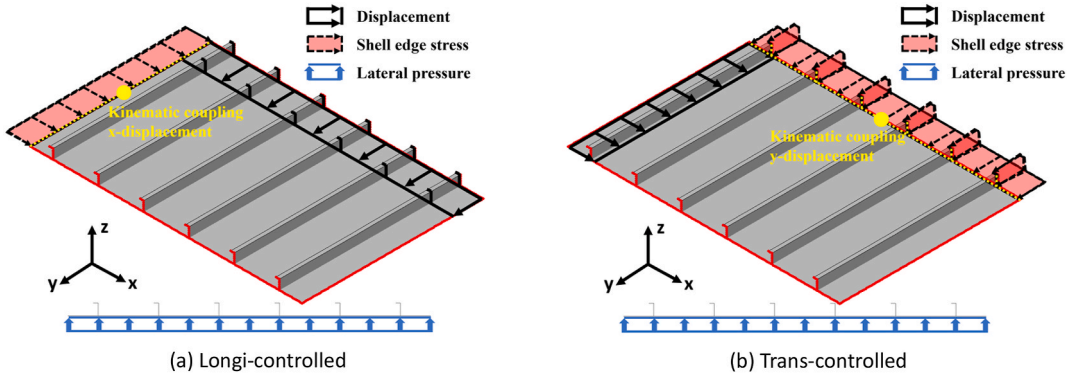

Fig. 4. Illustration of loading scenarios.

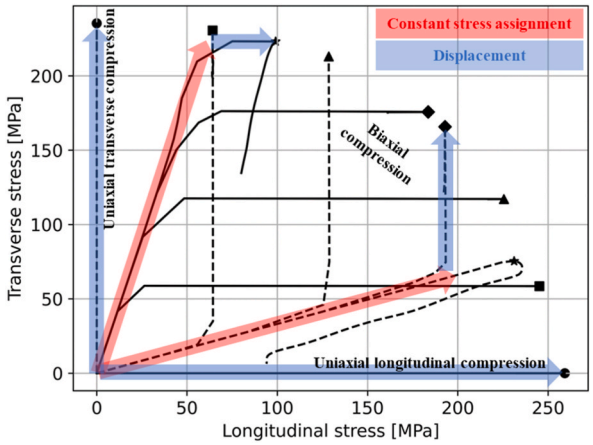

Fig. 5. Loading path curves of example cases. Longi-controlled and *trans*-controlled cases are plotted with solid and dashed curves, respectively.

reference experiments by Aalberg et al. [53]. The same failure modes and less than 15 % deviation from experimental ultimate strength values were obtained.

Geometrical imperfections were imposed by moving the nodes to the assumed displacement fields, including local plate deflections, global panel deflections and stiffener sideway distortions. The displacement fields were assumed to be sinusoidal and linear extrapolations as shown in Fig. 7. The wave number for plate deflection in the longitudinal direction depend on the plate aspect ratio as:

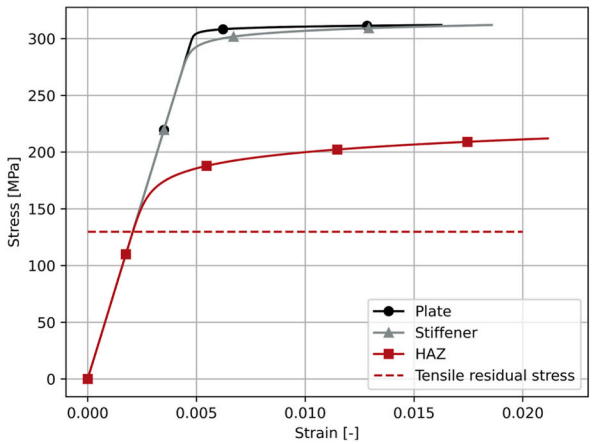

Fig. 6. Stress-strain curves of assumed materials.

Table 2
Material parameters [53].

	E [MPa]	σ^0 [−]	n [−]	α [−]
Plate	62612	309	179	0.405
Stiffener		302	58.8	0.415
HAZ		185.41	16.3	0.678

$$\left(\frac{sm}{l}+\frac{l}{ms}\right)^2 \geq \left(2\sqrt{\frac{sm}{l}\bullet\frac{l}{ms}}\right)^2 \tag{5}$$

, where l is the length of the plate between transverse frames, s is the width of the plate between longitudinal stiffeners, and m is the number of half sinusoidal waves in the longitudinal direction.

The local plate deflection amplitude A_{loc}, global panel deflection amplitude A_{glo}, and stiffener sideway distortion amplitude A_{stf}, were determined based on the DNV–OS–C401 Fabrication and Testing of Offshore Structures [55] as:

$$A_{loc} = 0.005s \tag{6}$$

$$A_{glo} = 0.0015l \tag{7}$$

$$A_{stf} = 0.0015l \tag{8}$$

The obtained longitudinal wave numbers and imperfection amplitudes are given in Table 3. It is believed to be conservative for aluminium ship structures. The aspect ratio φ, plate slenderness parameter β_p and reduced slenderness ratio of beam-column λ are also shown in the table. They are calculated based on the following equations. It is noticed that the slenderness parameters are rather large due to a small Young's modulus of aluminium alloys compared to steel structures.

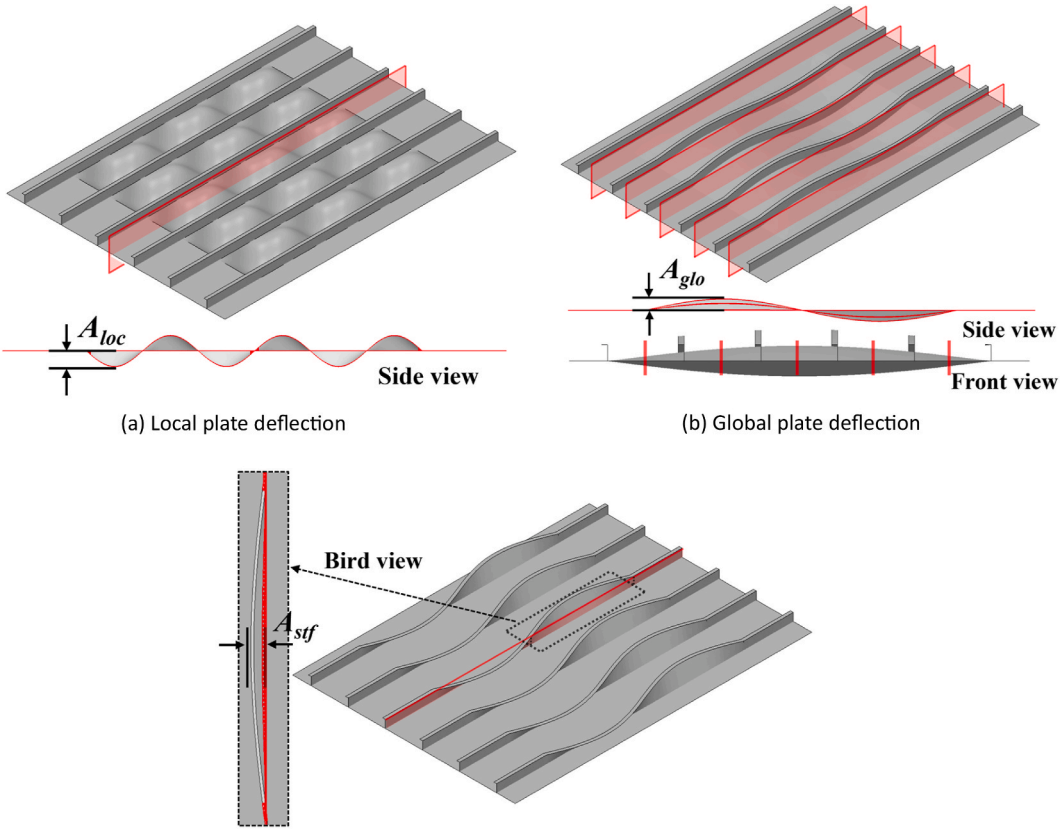

Fig. 7. Assumed imperfection fields. The deformation is displayed with a magnification factor of 10.

$$\varphi = l/s \tag{9}$$

$$\beta_p = \frac{l}{t}\sqrt{\frac{\sigma_y}{E}} \tag{10}$$

$$\lambda = \sqrt{\frac{\sigma_y}{\sigma_E}} \tag{11}$$

where σ_E is the Euler buckling stress of the beam-column.

The imperfections were only introduced into two complete spans to limit the failure position. This assumption was deemed acceptable after comparing it with simulations that incorporated imperfections over the entire model. The imperfection field in the outer half span doesn't influence the failure mode and ultimate strength.

The softened material and residual stresses were modelled to capture the HAZ effects. HAZ sizes and softening magnitudes could depend on the welding method, but the same values were assumed for butt and fillet welding in this work. This is consistent with the design rules. In all cases, the plate-frame-stiffener intersection welding was modelled. Either butt welding between extruded components or fillet welding between stiffeners and plates were modelled. The width of HAZ was taken as 40 mm as shown in Fig. 8, based on the experimental measurement by Rønning et al. [56] and a previous parametric study [20]. The residual stresses were modelled by pre-defined constant stress fields. The tensile residual stress level was 70 % of the HAZ yield stress, and the compressive residual stresses outside HAZ were assumed to balance. Only the stresses in the welding direction were modelled because the magnitude in other directions were found small in practice [57].

3.3. Other setups

The numerical simulations were carried out using the NLFEM software Abaqus. The 'Dynamic, Implicit' solver was chosen with its sub-option 'Quasi-static' [52]. Contrary to the 'Static, Riks' solver, this technique includes the inertia effects, which helps to overcome numerical instabilities in buckling simulations. In a natural time scale, the solution should be nearly the same as a truly static solution. No damping or strain-rate effects of the material are considered, and the loading rate is adjusted by test runs to avoid structural dynamic responses. The solver successfully predicted the uniaxial ultimate strength of aluminium stiffened panels in previous works [16,20].

The NLFEM models were meshed with linear quadrilateral element with reduced integration. Convergence studies were conducted to determine the mesh size. The stress-strain curves and vertical deflection contours at the ultimate strength point are compared in Fig. 9. Various mesh sizes produced similar failure modes and load end-shortening curves. For the *trans*-controlled 1000 mm panels, the difference of the ultimate stress was largest, and the deflection direction of one span changed with mesh sizes as noted by arrows. Nonetheless, the ultimate stress difference was within 5 % compared to the finest mesh. Thus, a mesh size of 10 mm was chosen to balance simulation accuracy and computation time.

In total 360 cases were simulated considering different panel lengths, welding patterns, loading conditions and load levels as summarized in Table 4. The notations in the table are used for naming the cases throughout the paper. For example, 'L400BuLoS25P0' represents a case with the panel length of 400 mm, butt welding pattern, longitudinal-displacement-controlled, a constant transverse stress of 25 % uniaxial ultimate strength, and no lateral pressure.

4. Numerical results

4.1. Force end-shortening curves

Figs. 10 and 11 plot the force end-shortening curves in the main loading direction, i.e., the displacement-controlled direction. The load end-shortening curves of the longi-controlled cases (solid lines) increases almost linearly until the peak load is reached, and this is followed by a sudden capacity loss. With increasing transverse pre-stresses, the peak load carrying capacity decreases, while the slope remains virtually the same. Buckling/yielding of stiffeners dominates in these cases.

In the *trans*-controlled cases (dashed lines), the load end-shortening curves exhibit a nonlinear stage before reaching the peak capacity, followed by a capacity loss. Elevating longitudinal pre-stresses in these cases leads to earlier and faster nonlinear stage progression, substantially reducing the peak. The failure is governed by local plate buckling. Prior to buckling, the plates between stiffeners exhibit linear responses. In the post buckling stage, the load carrying capacity continues to increase due to the effects of

Table 3
Initial imperfection parameters.

l [mm]	φ [−]	β_p [−]	λ [−]	m [−]	A_{loc} [mm]	A_{glo} [mm]	A_{stf} [mm]
400	1.33	2.62	0.45	1	1.5	0.6	0.6
600	2	3.94	0.68	2	1.5	0.9	0.9
800	2.67	5.25	0.91	3	1.5	1.2	1.2
1000	3.33	6.56	1.13	3	1.5	1.5	1.5

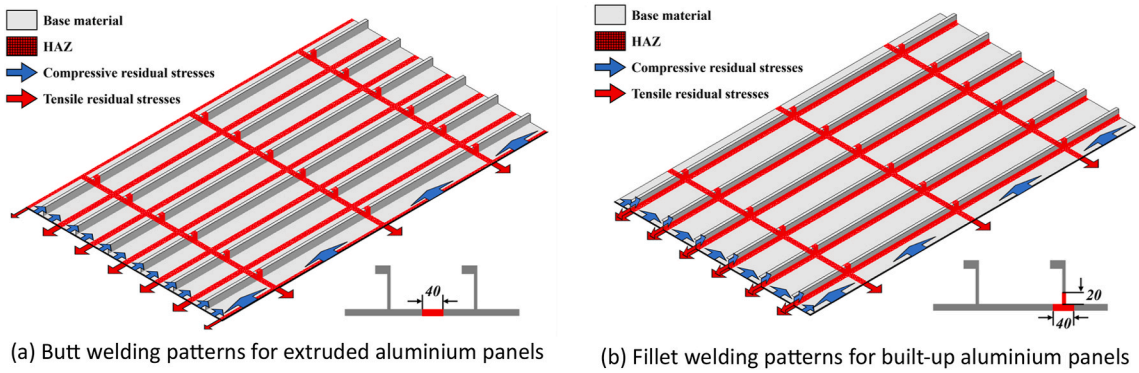

(a) Butt welding patterns for extruded aluminium panels (b) Fillet welding patterns for built-up aluminium panels

Fig. 8. Illustration of HAZ and residual stresses.

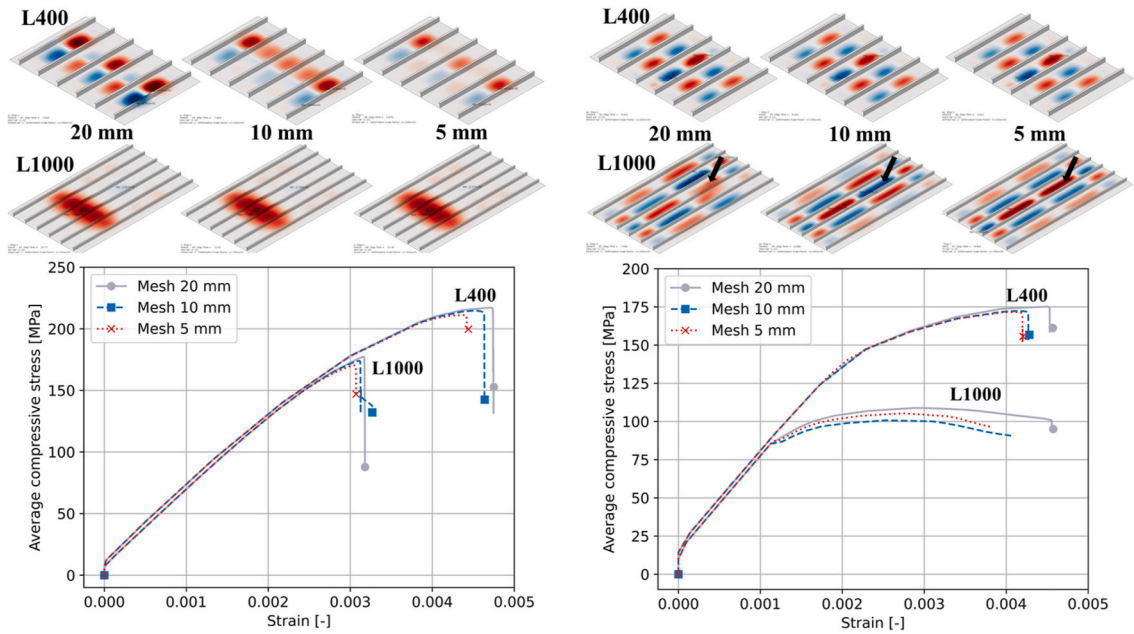

(a) Longi-controlled cases (b) Trans-controlled cases

Fig. 9. Results of mesh size convergence tests.

Table 4
Simulation case definitions with different setting combinations.

Panel length	Welding pattern	Loading scenario	Orthogonal stress level	Lateral pressure
400 (L400)	No welding (No)	Longi-controlled (Lo)	0 (S0)	0 (P0)
600 (L600)	Butt welding (Bu)	Trans-controlled (Tr)	25 % (S25)	0.1 (P10)
800 (L800)	Fillet welding (Fi)	–	50 % (S50)	0.2 (P20)
1000 (L1000)	–	–	75 % (S75)	–
–	–	–	95 % (S95)	–

constrained edges. Pronounced nonlinear responses emerge with nonlinear materials and geometries. The structures lose their capacity progressively until a collapse point.

Observations with respect to the force end-shortening curves are listed as follows.

- For a slenderer panel, the longitudinal load carrying capacity decreases, while the transverse load carrying capacity increases due to a larger section area in the transverse direction, even though stress values decrease. Thus, the L400 cases have higher

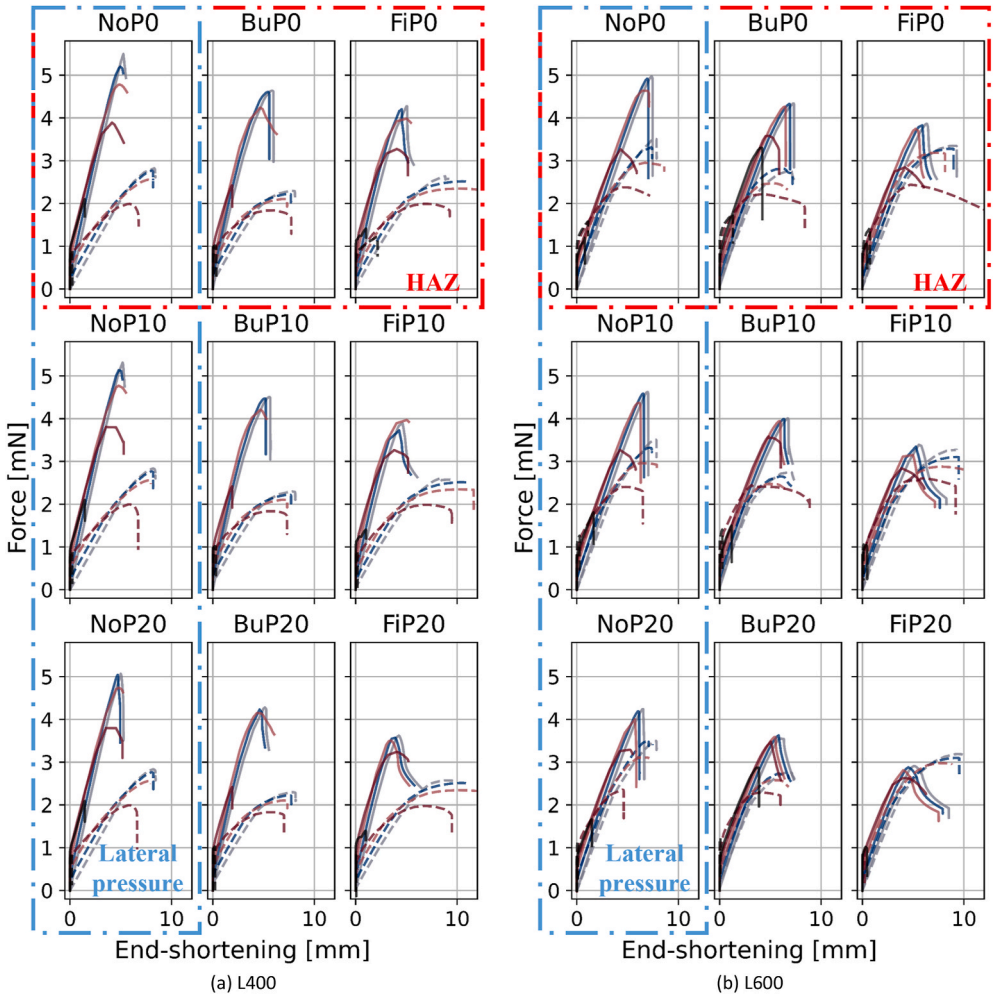

Fig. 10. Force end-shortening curves of axial compression (solid lines) and transverse compression (dashed lines) in L400 and L600 cases. Darker colour represents larger orthogonal stresses (0, 25 %, 50 %, 75 % and 95 %).

longitudinal capacity curves than transverse capacity curves; the L600 cases have almost overlapping capacity curves; and the L1000 cases have higher transverse capacity curves.

- The presence of lateral pressure substantially reduces the longitudinal load carrying capacity, particularly for slender panels, as they experience higher bending stress. The introduced lateral pressure has little influence on the transverse load carrying capacity, with the exception of the slenderest L1000 cases. This can be attributed to the change in the number of transverse half-waves, as displayed in the left most patterns of L1000 cases in Fig. 13-b. The lateral pressure generates a failure pattern with local buckling between each stiffener, while there are only three half-waves in the case without the lateral pressure, i.e., the stiffeners 'participate' in the deflections. Less transverse force is needed for the former pattern to trigger local plate collapse due to a critical half-wave number.
- Generally, the longitudinal load carrying capacity is more influenced by fillet- than butt welding, while transverse capacity is more influenced by butt- than fillet welding. The influence is mainly related to the overlap between the highly stressed area and the softened HAZ [20]. In the fillet welding cases, it is noticed that the transverse capacity curves (dashed lines) have larger displacement subjected to the same force level. The reason could be that the softened stiffener-plate intersection in these cases yields earlier and behaves like a hinge, so the local plate tends to deflect, resulting a larger in-plane shrinkage.

4.2. *Failure modes*

The failure modes of the stiffened panels are often quite complex and may involve several deformation components. It is, however, possible to distinguish between four main categories.

(1) Global collapse with asymmetric stiffener buckling.

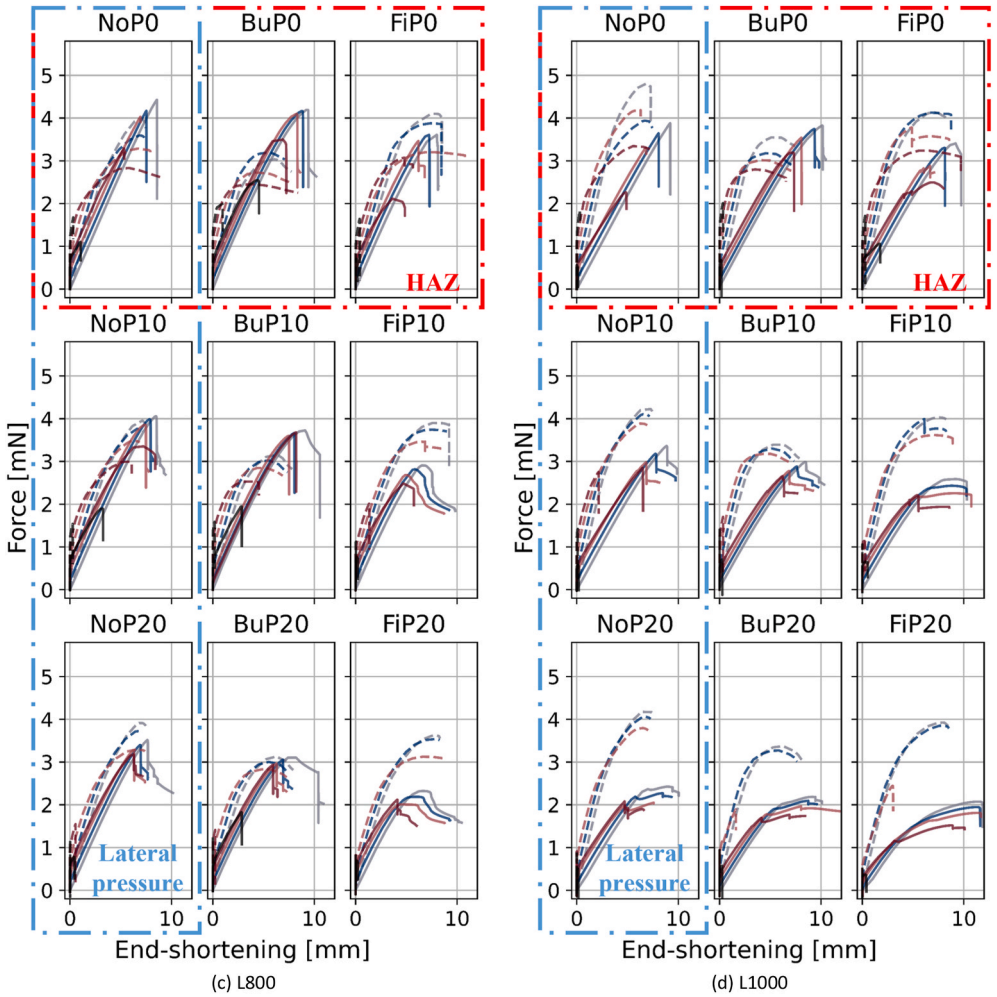

Fig. 11. Force end-shortening curves of axial compression (solid lines) and transverse compression (dashed lines) in L800 and L1000 cases. Darker colour represents larger orthogonal stresses (0, 25 %, 50 %, 75 % and 95 %).

(2) Global collapse with symmetric stiffener buckling.
(3) Local plate buckling induced collapse.
(4) Mixed collapse mode

Several sub-modes exist depending on the involved number of stiffeners or half-waves. The failure modes in selected cases are illustrated schematically in Fig. 12, which displays the vertical deformations at the ultimate strength point.

Mode 1 represents the collapse mode induced by asymmetric stiffener buckling. In this mode, the panel exhibits a beam-column buckling behaviour, with upward deformations in one span and downward deformations in the adjacent span, which are often accompanied by stiffener tripping. This failure mode occurs with dominant longitudinal compression without lateral pressure. When transverse stresses are assigned, the panel may develop several half-waves in the transverse direction as shown in Mode 1–2, but the half-waves are still asymmetric about the frames.

Mode 2 represents the symmetric stiffener buckling induced collapse. In this mode, both spans are subjected to beam-column failure with upward deformation. The failure mode occurs notably with large lateral pressure and predominant longitudinal stresses. When the transverse stresses become significant, more half-waves develop in the transverse direction as shown in Mode 2-1 and Mode2-2. In the L1000NoTrS75P10 (Mode 2-2) case, indicated by yellow arrows, downward deformation is observed in a single span, whereas in the L1000NoTrS50P20 (Mode 2–3) case, the phenomenon occurs in both spans. The reason is that in the former case (Mode 2-2), larger constant longitudinal stresses suppress the influence of transverse stresses.

Mode 3 represents the plate buckling induced collapse. In this mode, several half-waves develop in the transverse direction with asymmetric shape about stiffeners. This failure mode appears for predominant transverse stresses. The applied lateral pressure in Mode 3-3 generates a symmetric deformation pattern about transverse frames as noted by green arrows. It is noticed that Mode 3-2 have fewer transverse half-waves. This deformation pattern indicates a development of global failure mode that is induced by transverse

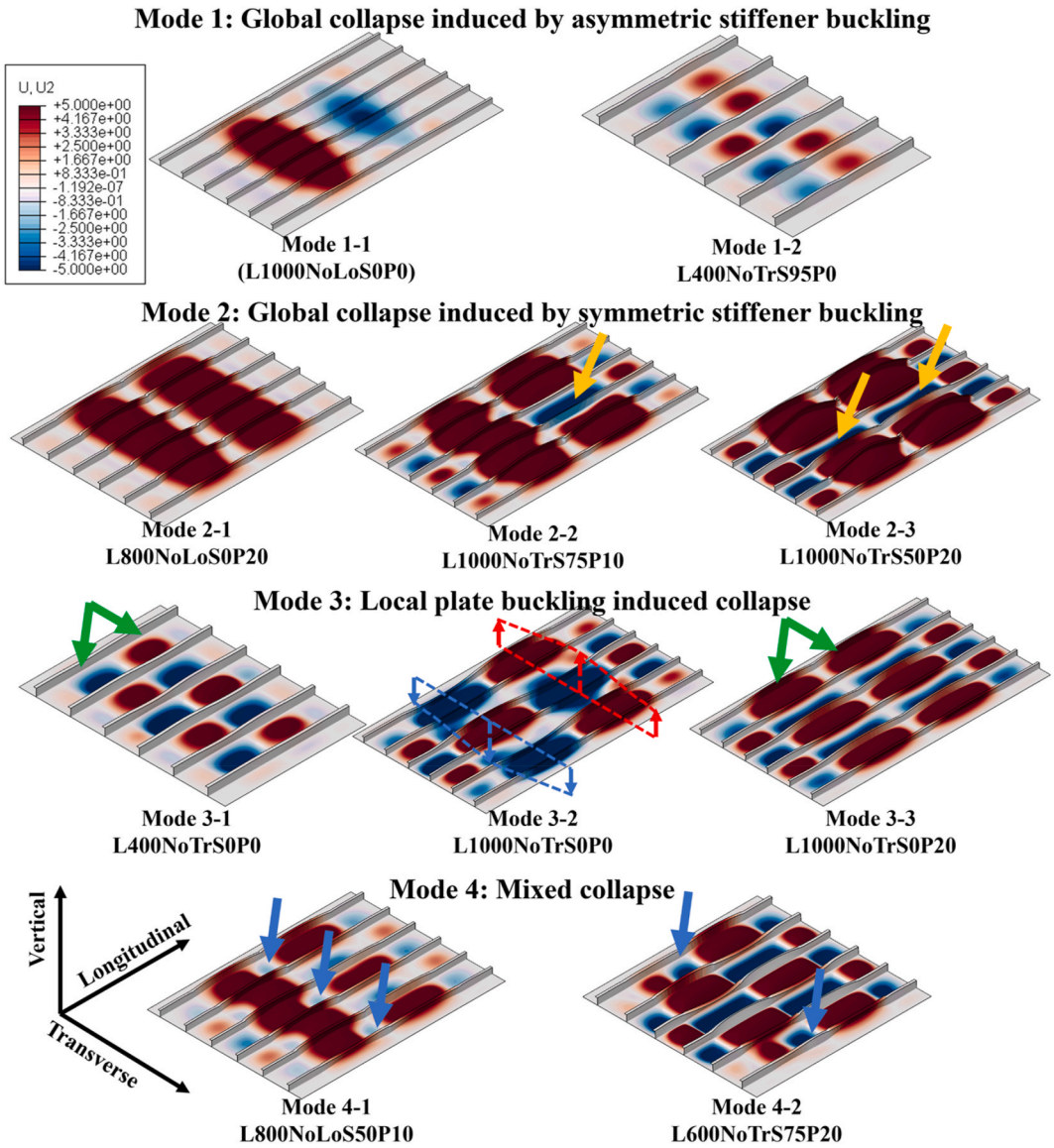

Fig. 12. Schematic illustration of the failure modes. The deformation is displayed with a magnification factor of 10.

stresses. It is believed that this mode as sketched in Mode 3-2 could be generated by further increasing the panel length.

Mode 4 represents the mixed collapse mode with combined local plate and stiffener buckling. In this mode, the local plate buckling dominates in one span while the stiffener buckling appears in the other. This failure mode happens with comparable longitudinal and transverse stresses. As noted by blue arrows, downward deformations of local plate can happen in a small area together with the stiffener beam-column buckling. They are triggered by large transverse stresses.

The panel vertical deformations at the ultimate strength point are displayed with a bird's-eye view in Figs. 13 and 14 with L400 and L1000 cases. From the left to the right, the loading scenario changes from uniaxial transverse compression to uniaxial longitudinal compression. Lateral pressure increases from the top to the bottom in Fig. 13. Fig. 14 considers different welding patterns with no lateral pressure applied.

The failure processes depend on the loading scenarios. When longitudinal stresses are dominant, the frame-stiffener intersections yield first. This doesn't, however, represent the ultimate strength of the structure, and the load end-shortening curves continue to increase. The stiffeners are subjected to strong bending moments. Final collapse is triggered either by further development of the yield zones at the stiffener ends or material yielding at the stiffener mid-span. This is also found when transverse frames are physically modelled [45]. The failure process is typical for aluminium stiffened panels. When transverse stresses are large, plate buckling induced collapse dominates. The yield area develops mainly along the plate mid.

Observations with respect to the failure modes are summarized as follows.

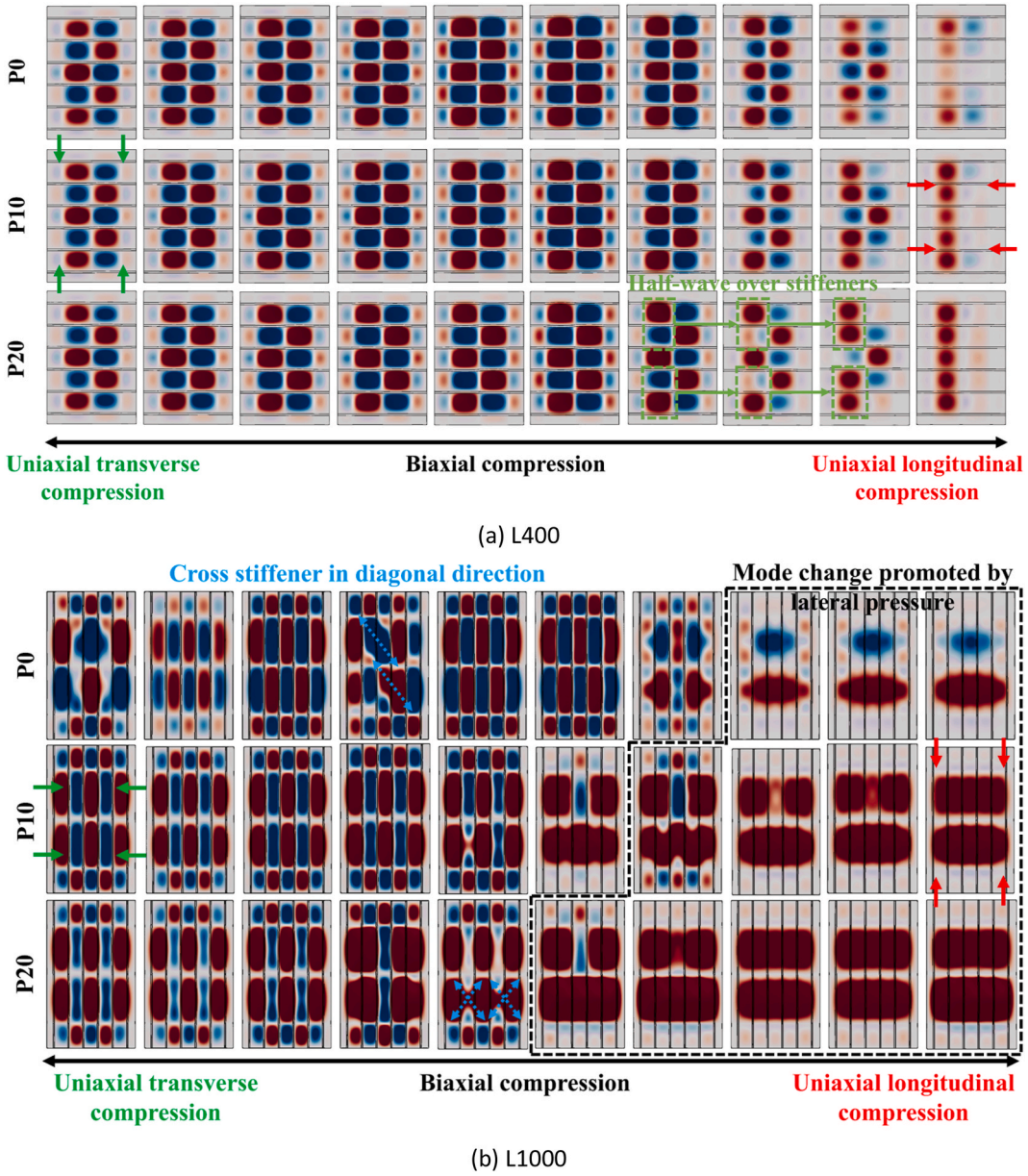

Fig. 13. Vertical deformation at ultimate strength point with different lateral pressure levels; Red: upward deformation; Blue: Downward deformation; L1000 cases are rotated 90° for better figure arrangement. Green and red arrows show uniaxial loading directions.

- Transverse stresses tend to induce alternating half-waves between stiffeners in the transverse direction. The half-wave length can however, span over several stiffeners when longitudinal stresses become large as shown in in Fig. 13-a. Beam-column buckling or stiffener tripping tend to occur in these cases. As marked by blue arrows in Fig. 13-b, shear effects from biaxial compression results in half-waves that are across stiffeners in the diagonal direction.
- Lateral pressure promotes symmetric buckling patterns in both stiffener and plate induced collapse. In addition, lateral pressure facilitates half-waves across stiffeners as if there are larger longitudinal stresses. This phenomenon can be observed by the marked L1000 cases within the dashed lines in Fig. 13-b. In these cases, symmetric stiffener buckling (Mode 2) replaces asymmetric stiffener buckling (Mode 1) and local plate buckling (Mode 3) with a larger lateral pressure even though the longitudinal stresses are smaller.

4.3. Ultimate strength

The panel ultimate strength is taken at the peak point of the load-displacement curves. The calculated ultimate strength for

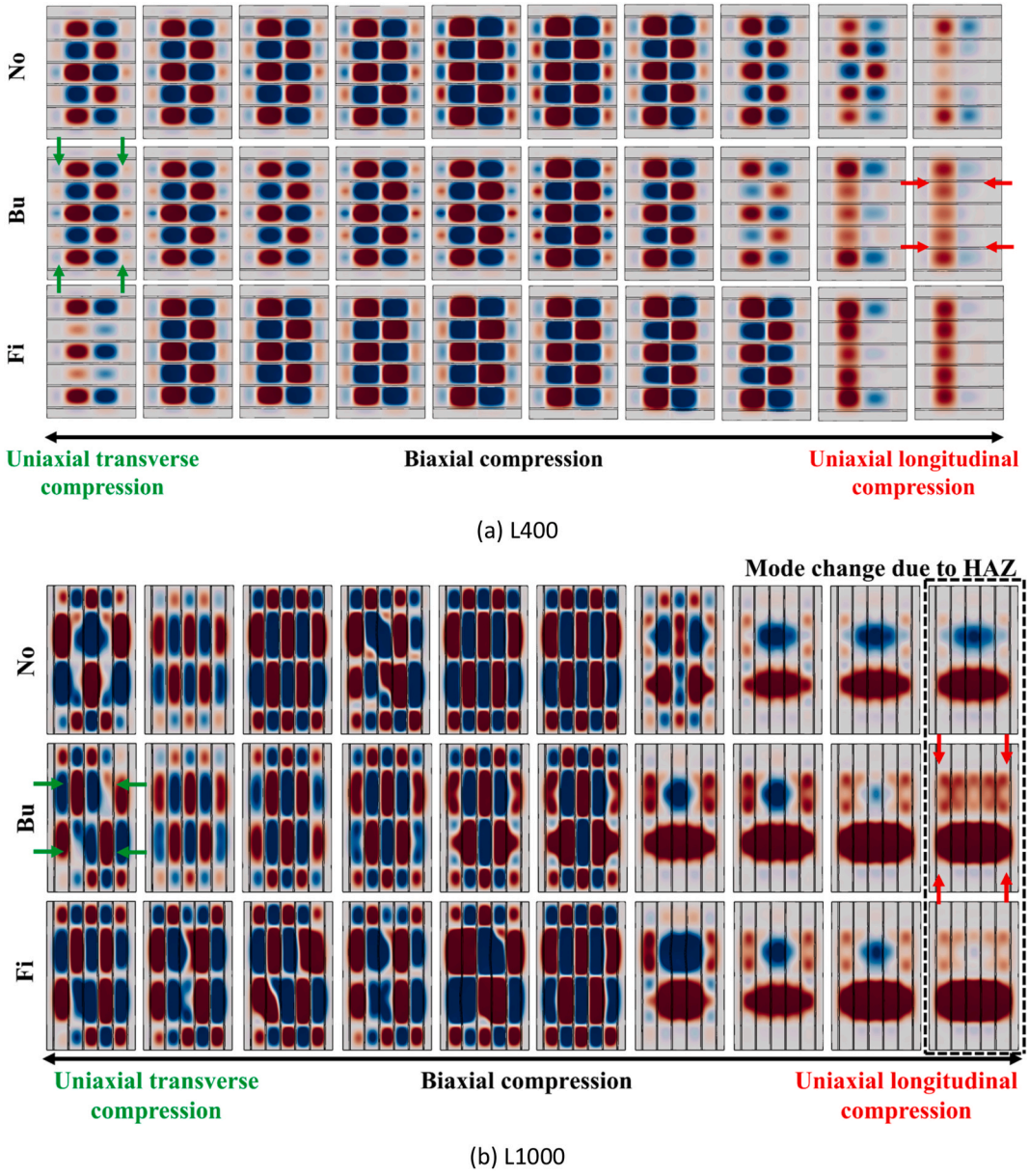

Fig. 14. Vertical deformation at ultimate strength point with different welding patterns; Red: upward deformation; Blue: Downward deformation; L1000 cases are rotated 90° for better figure arrangement. Green and red arrows show uniaxial loading directions.

- Welding HAZ doesn't change the failure mode in most cases. Only when a slender panel is subjected to large longitudinal stresses, as marked with the dashed lines in Fig. 14-b, the asymmetric stiffener buckling (Mode 1) changes to the symmetric mode (Mode 2). The softened material in HAZ weakens the stiffener or the attached plate, thus promoting the upward deformation.
- When transverse stresses are large or the two stress components are comparable, HAZ only alters the failure mode between different sub-modes, by changing half-wave numbers or symmetry. However, recalling that the observed force end-shortening curve change due to the welding patterns, it is interesting to notice that such changes can possess substantial difference with respect to the structural response.

combined loads are plotted in terms of the longitudinal and transverse stresses in Figs. 15 and 16. The values are normalized by the plate yield stress (309 [MPa]). The normalized von Mises yield stress contour for parent- and HAZ yield stress is also plotted for reference. The cases with the lateral pressure of 0, 0.1 and 0.2 MPa are presented in grey, blue and red, respectively. Comparing sub-figures, such as Fig. 15-a, -c and -e for L400 cases, can trace the influence of welding patterns.

The following observations are made.

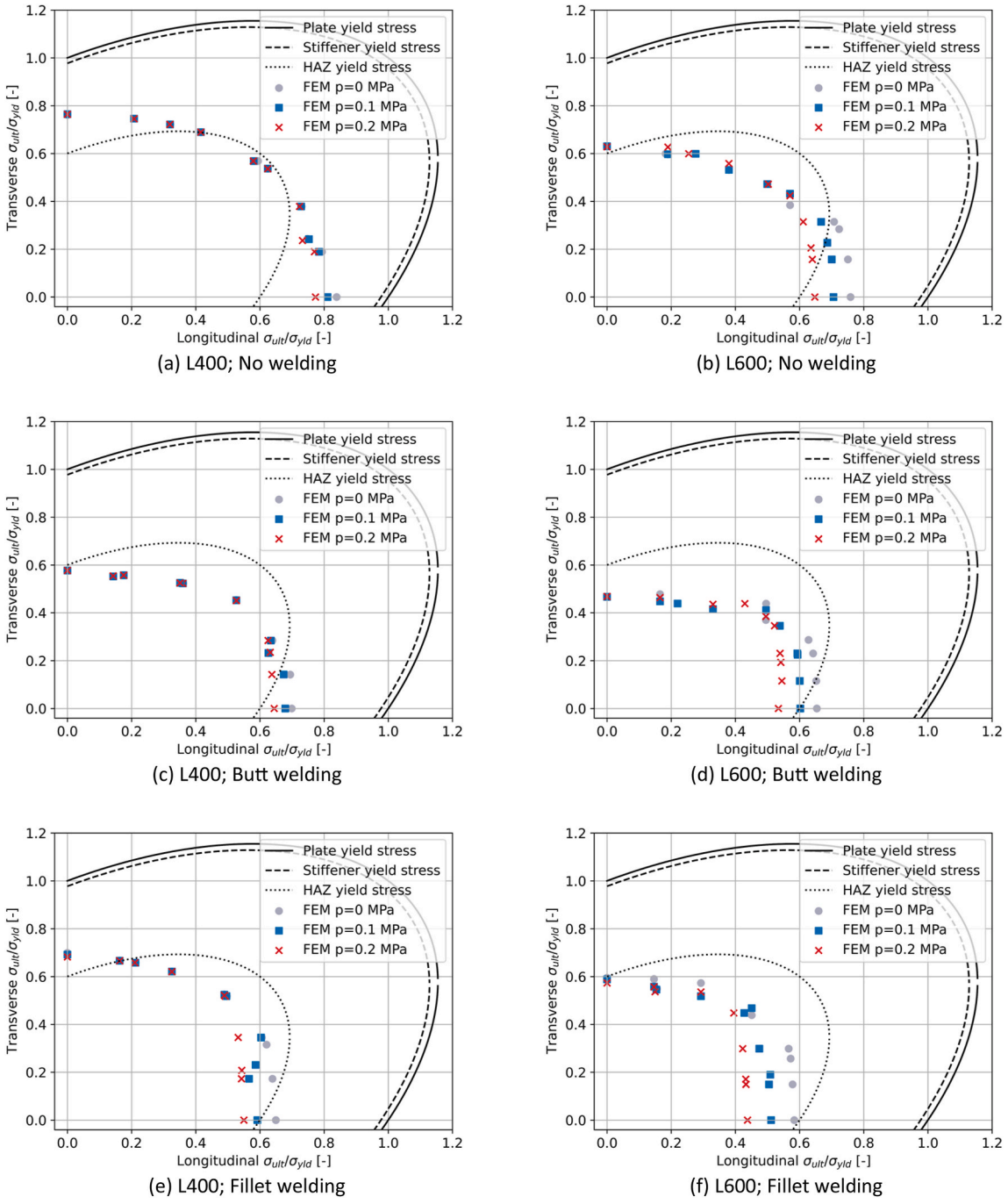

Fig. 15. Normalized ultimate strength in L400 and L600 cases.

- The ultimate strength points are within the HAZ yield stress criterion in most cases. When longitudinal stresses predominate, the ultimate strength may be larger than the HAZ criterion for stocky panels such as L400 and L600 case. Increasing the panel length generally decreases the ultimate strength due to interframe buckling.

- Lateral pressure tends to reduce the ultimate strength when longitudinal stresses predominate, mainly due to a shift in the stiffener failure mode from asymmetric (Mode 1) to symmetric (Mode 2). When transverse stresses are large, the reduction of the ultimate strength from the lateral pressure is minor, suggesting that different sub-modes (Mode 3-1, Mode 3-2 and Mode 3-3) of local plate buckling influence little on the ultimate strength.

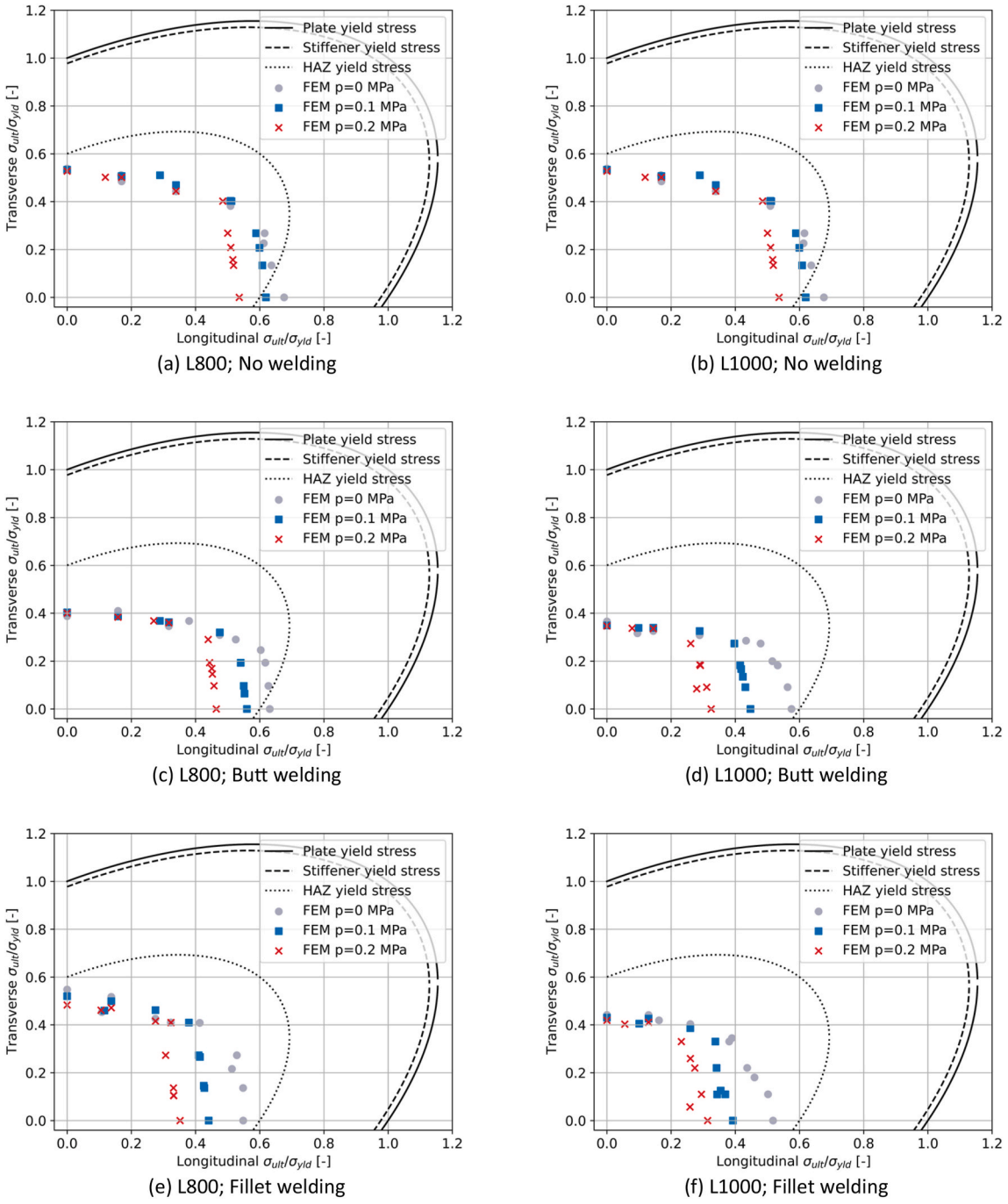

Fig. 16. Normalized ultimate strength in L800 and L1000 cases.

- Butt welding (extruded profiles) reduces both the longitudinal and transverse ultimate strength. It produces softened material in the mid-plate. In longi-controlled cases, the softening deteriorates the capacity of stiffener plate flange to some extent. The material yields prior to plate buckling, causing a capacity reduction, even though the HAZ (mid-plate) is little stressed in the post buckling stage. In *trans*-controlled cases, the softening reduces the yielding stress of mid-plate directly, and the areas are highly stressed. As a result, it deteriorates the plate capacity substantially. Accordingly, a small longitudinal strength reduction and large transverse strength reduction can be observed due to butt welding.
- Fillet welding (built-up profiles) reduces the longitudinal ultimate strength mainly and influences the transverse ultimate strength little. The softened material at the stiffener-plate intersections significantly reduces stiffener capacity, leading to a reduction in

longitudinal strength. However, the softened areas have limited contribution to the plate failure when transverse stresses predominant.

4.4. Comparison with design methods

The numerical results are compared with predictions from the IACS rule (2018 version) and the PULS approach. In the design methods, no safety factors are applied, and the input material parameters and initial imperfections are adjusted to align with those in the numerical simulations. In the IACS rule, global panel deflection from the simulations is taken as assumed imperfection w_0 of the

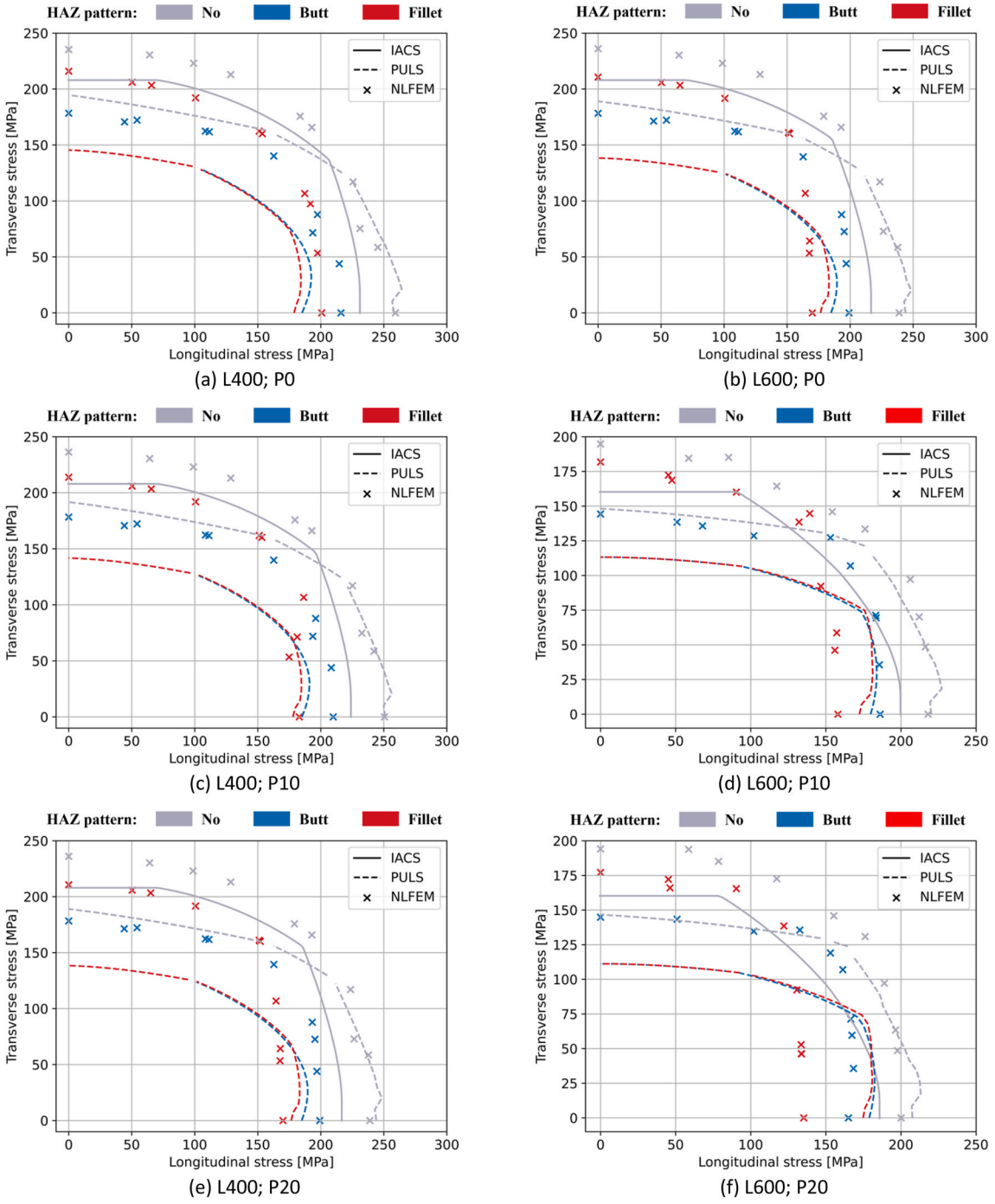

Fig. 17. Comparison between predictions of design methods and NLFEM results in L400 and L600 cases.

stiffener ultimate limit check. In the PULS approach, the local plate deflection, global panel deflection and stiffener sideway distortion are used as initial plate deflection, stiffener deflection and stiffener tilt in the PULS software, respectively. Welding effects are also included in the PULS by specifying the fabrication method. The 'welded' option corresponds to fillet welding and the 'extruded' option corresponds to butt welding. A material reduction factor of 0.6 in HAZ is used as input.

The panel ultimate limits predicted by the IACS rule (solid lines), the PULS approach (dashed lines) and the ABAQUS simulations (markers) are compared in Figs. 17 and 18. Different colours represent different welding patterns. It is essential to emphasize that the numerical simulation employed in this study are not perfect. While some deviation points are evident, the primary focus remains on assessing and comparing the overall trend.

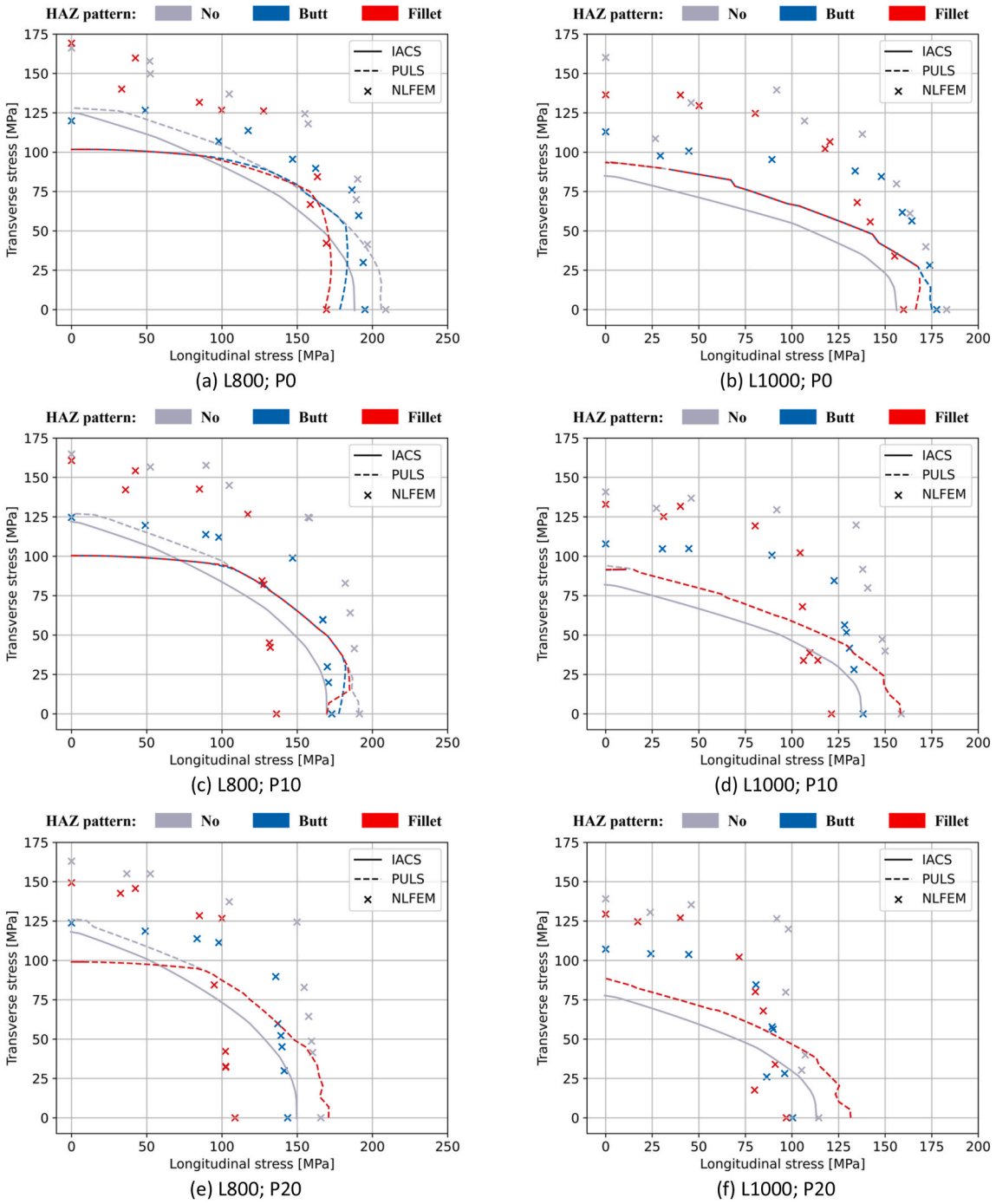

Fig. 18. Comparison between predictions of design methods and NLFEM results in L800 and L1000 cases.

The IACS rule does not account for welding patterns and consequently produces a single curve. The rule predicts reasonable ultimate strength for stocky panels compared to numerical simulations. The accuracy becomes worse for slender panels, especially for cases that are dominated by transverse loads. The PULS approach also gives a good prediction of ultimate limits when the welding effects are not included.

Regarding the welding effects, the ultimate limit of PULS predictions is notably influenced in the L400 and L600 cases, while the influence is limited in L800 cases, with little change in L1000 cases. This outcome may stem from the fact that, in these cases, the added yield criterion is not as critical as the default stiffener compression criterion.

For butt welded panels (extruded profiles), the PULS approach agrees well with the simulations. With lateral pressure, the ultimate limit can be unconservative for slender panels subjected to large longitudinal stresses, as shown in Fig. 17-f, Fig. 18-c, -d, -e and -f.

For fillet welded panels (built-up profiles), the PULS approach can give satisfactory predictions in all L400 cases. The ultimate limit of the L600, L800 and L1000 cases without lateral pressure can also be captured. With the presence of lateral pressure, the ultimate strength is over-predicted when longitudinal stresses predominate.

It has been observed that both design methods yield conservative predictions when transverse stresses are predominant. The IACS rule predicts improper failure modes in such scenarios, and Section 5.3 provides a comprehensive discussion and modification. The PULS approach deviates due to its assumption that failure occurs upon the first yielding of membrane stresses. However, after the first yielding of plates, a reserve capacity exists due to material nonlinearities, as validated by the nonlinear stage of the force end-shortening curves in Figs. 10 and 11 (dashed lines). This incomplete consideration of nonlinear effects within in the PULS approach leads to conservative predictions.

Fig. 19 shows the different failure categories in the IACS rule and the NLFEM results without the welding effects. Different colours represent different lateral pressure levels. For the stocky panels (L400), the numerical results approach the plate buckling limit with large longitudinal stresses. For the slender panels (L1000), the numerical results are close to the stiffener yielding limit. It reveals that the practical failure mode for the stocky panels combines both the stiffener and plate buckling, while the beam-column buckling is more critical for the slender panels. Considering that the design methods normally take the most critical one among different failure categories, the predictions can be very conservative in some cases. For example, in the L1000 cases, the stiffener buckling/yielding

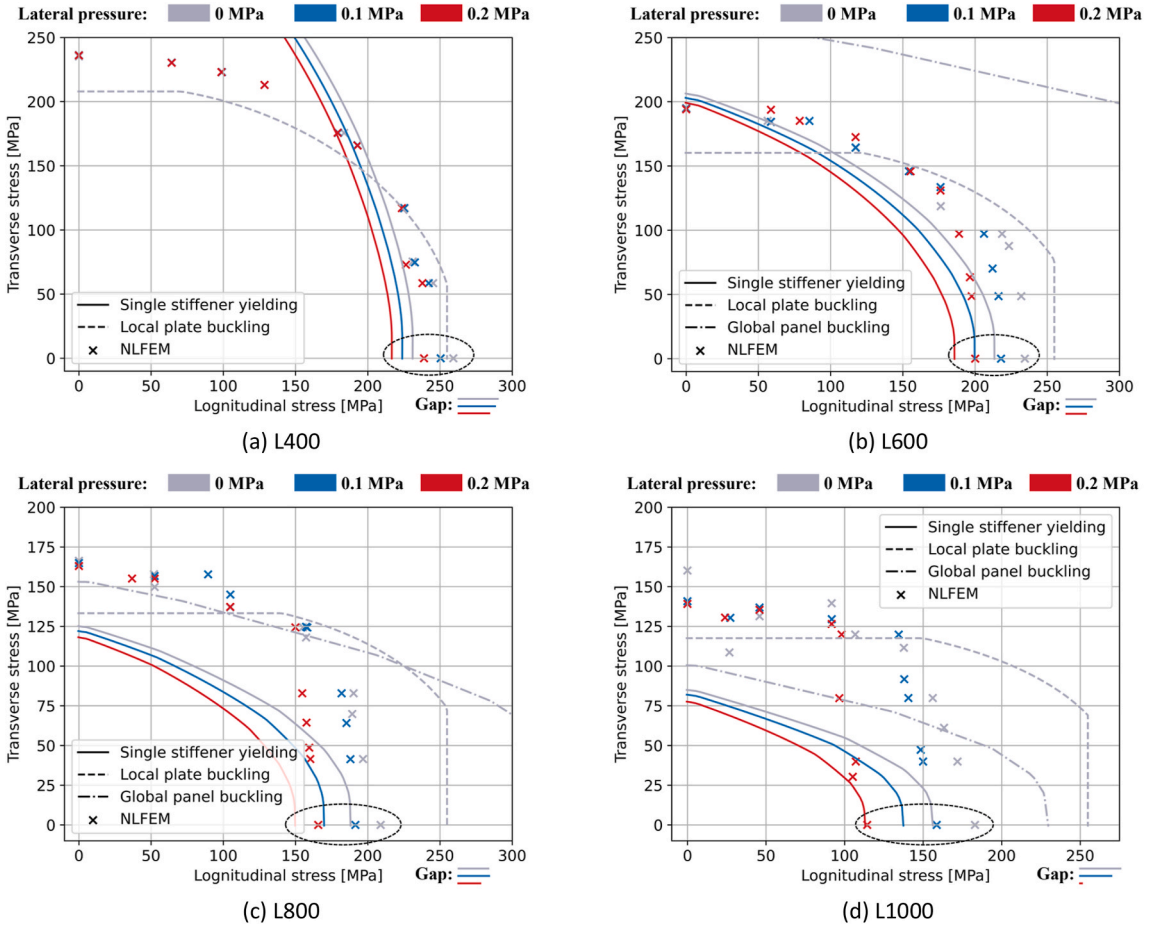

Fig. 19. Failure categories of the IACS rule and NLFEM results under different lateral pressure.

category predicts only around half of the transverse capacity from the numerical simulations. The local plate buckling/yielding category agrees better with the numerical failure patterns and will be more accurate to predict the transverse ultimate strength in this case.

5. Discussion

5.1. Lateral pressure effects

Given a proportional loading path, as discussed in Section 3.1, Fig. 20 illustrates correlations between design method predictions and NLFEM results. The mean value reveals an averaged ratio between design method predictions and the NLFEM results. A value smaller than one means a general conservative prediction from the design methods. The coefficient of variance (COV) shows the extent of variability in relation to the mean value. Different colours represent different lateral pressure levels.

When welding effects are not included, the IACS rule is more conservative than the PULS approach as shown by the mean values in Fig. 20-a and -b. Both the mean value and the COV increase with a higher lateral pressure in both methods, indicating reduced conservatism and greater variability.

In the presence of welding effects, the predictions from the PULS approach agree well with the NLFEM simulations for the mean values. This reveals that adding yielding criteria in the HAZ could help to include welding effects for aluminium stiffened panels. Nonetheless, the conservative of the PULS approach reduces substantially with increased lateral pressure, notably in the fillet welded cases. The COV also increases substantially in this case. It indicates that the interactions between the fillet HAZ and lateral pressure are not fully included in the method.

As shown in Fig. 19, the stiffened panel buckling limit and local plate buckling limit in the IACS rule are not influenced by the lateral pressure, while the single stiffener yielding limit reduces. This is because equation (1) and equation (2) in Section 2.1 do not include the lateral pressure. Although the single stiffener yielding limit reduces with a larger lateral pressure, the gap between the numerical results and the limit becomes smaller, which suggests a reduced conservative in the rule. This phenomenon is because that

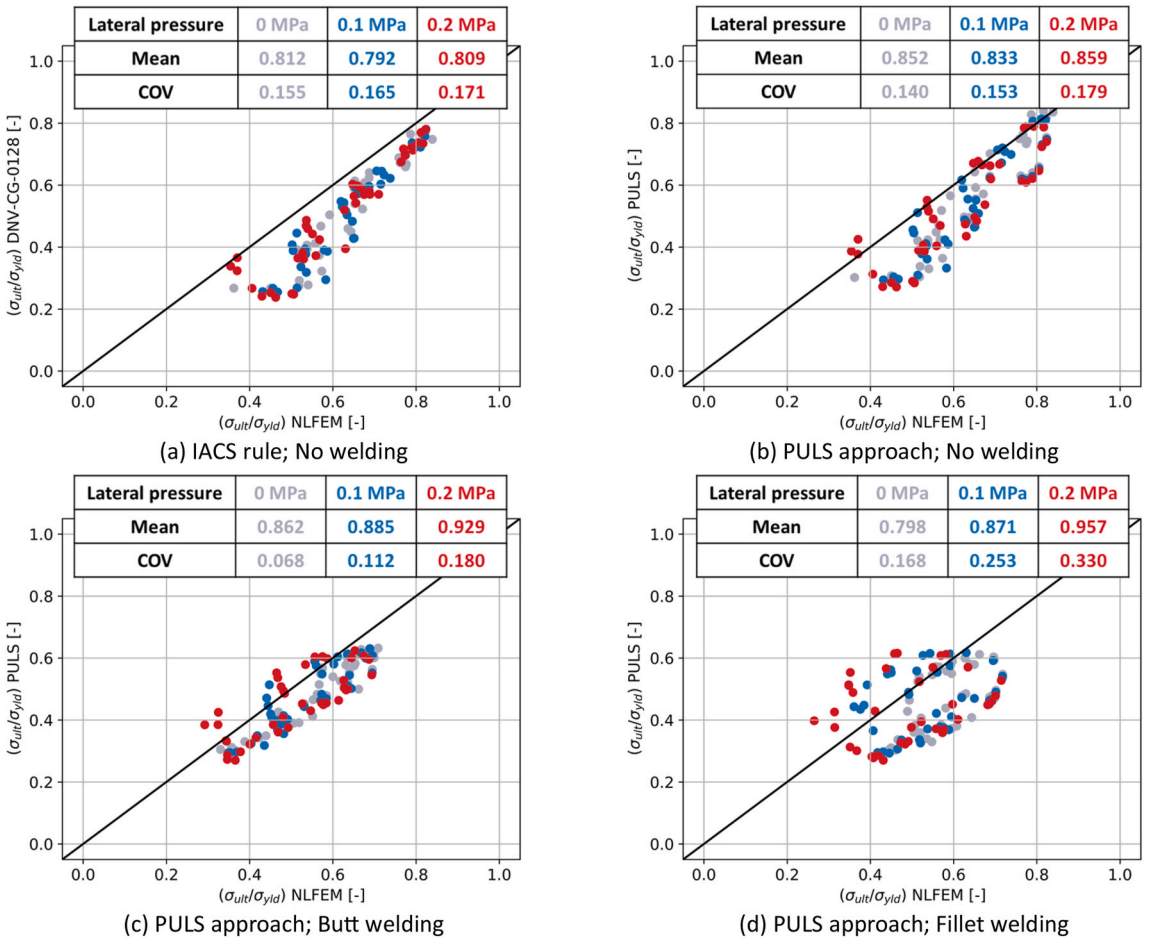

Fig. 20. Correlations between design method predictions and NLFEM results.

the nonlinear global effects are significant for aluminium structures [42] and that such global deformation is not fully considered in the design method mainly for steel structures.

In the IACS rule, stiffener ultimate strength is characterized by yielding of the single stiffener subjected to axial, bending and torsional stress as shown in equation (3). The lateral pressure is factored in the calculation of the bending stress, and there are two bending moment contributions. One is the contribution directly from the lateral load. The other is from the lateral deformation of the stiffener subjected to axial loads. This deformation is magnified based on the overall stiffened panel deformation, disregarding the lateral pressure. For steel structures, this assumption may be reasonable, but it may be unconservative for aluminium. The overall stiffened panel deformation of aluminium structures can be critical when the lateral pressure is large and/or the panel is slender, thus resulting in additional bending moment to the stiffener.

Further research is needed to understand the lateral pressure effects on the global panel failure of the aluminium structures. The sensitivity should be considered in both the local plate and global panel evaluation in the IACS rule. A complete consideration of the effects contributes the accuracy of the global stiffened panel limit and keep constant conservative of the single stiffener yielding limit.

As a summary, both methods can be used to predict the ultimate strength of aluminium stiffened panels under the biaxial compression, but modification related the lateral pressure influence is still needed.

5.2. Failure categories

The PULS approach encompasses six failure categories, as detailed in Section 2.2. In a similar manner, the IACS rule has four failure categories corresponding to category (2)–(5). The additional yielding categories in the PULS approach make it possible to include welding effects. To validate the assumptions of the PULS approach, the predicted critical category is compared with numerical results.

The PULS approach use the first yielding criterion, while the stiffener-frame intersections yield first in most simulations, which is not critical for the ultimate strength evaluation. Also, there can be several positions yielding simultaneously. Thereby, it is assumed that a consistent prediction of critical failure categories fulfils the following conditions.

- Numerical yielding area at the ultimate strength point includes the critical position predicted by the PULS approach.
- Stress state (compression or tension) predicted by the PULS approach matches the numerical result.

The percentage of consistent critical category is presented in Table 5.

The critical category predicted in the PULS approach coincides well with most numerical results. After imposing the welding effects, the agreement gets better. The change of the failure position due to HAZ effects can be well captured by the PULS approach. With an increasing slenderness and increasing lateral pressure, the disagreement between critical category increases. The discrepancies arise from opposite deflections of the stiffened panel, which result in a varying stress state.

Fig. 21 shows an example of inconsistent predictions. In this distance, the PULS approach identifies the compressed stiffener sides (with downward deformation) as the failure position, whereas simulations reveal the tensioned stiffener side (with upward deformation) for both complete spans. It's worth noting that the deformation pattern at span no.2 may resemble the PULS result in shape, but the magnitude of the downward deformation significantly deviates from the PULS prediction. This once again addresses that the overall deformation of the aluminium stiffened panels is not well captured in the compared design method.

5.3. Potential improvements of the IACS rule

- **Transverse load effects**

Results from Fig. 18 showed that predictions from the IACS rule were overly conservative when transverse stresses predominate. The predicted ultimate strength can be approximately half of the values obtained from numerical simulations in some cases**.** The design rule suggests the stiffener yielding failure mode predominates, while simulations show different failure modes, notably governed by local plate bucking/yielding, and even suggest the potential for global plate buckling. In view of the large discrepancies, the design rule can be overly conservative and questionable for panels loaded by predominant transverse compression.

In the original IACS rule, the effect of transverse loads is transformed into an equivalent virtual longitudinal load based on global panel buckling theory, and this virtual load produces the bending moment M_0 that contributes to the stiffener yielding as:

Table 5
Percentage of consistent critical category.

	P0	P10	P20	P0	P10	P20
		L400			L600	
No	100 %	90 %	70 %	80 %	60 %	60 %
Butt	100 %	100 %	100 %	100 %	100 %	100 %
Fillet	100 %	100 %	100 %	100 %	100 %	100 %
		L800			L1000	
No	70 %	<30 %	<30 %	60 %	<30 %	<30 %
Butt	70 %	90 %	40 %	40 %	<30 %	<30 %
Fillet	90 %	60 %	50 %	90 %	<30 %	<30 %

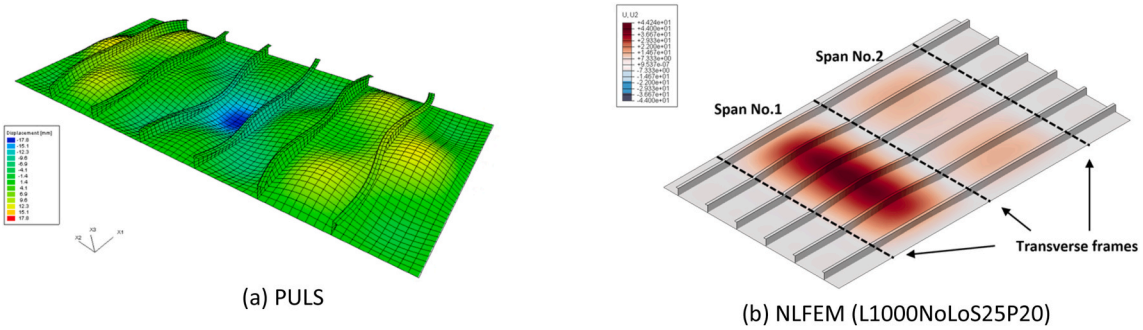

Fig. 21. An example of inconsistent predictions between PULS and NLFEM; Vertical deformations are displayed.

$$M_0 = F_E \frac{\gamma}{\gamma_{GEB} - \gamma} w_0 = F_E \frac{\gamma}{\gamma_{GEB}} \frac{1}{1 - \frac{\gamma}{\gamma_{GEB}}} w_0 \tag{12}$$

where F_E is the ideal elastic buckling force of the stiffener; γ is the stress multiplier factor for stiffener yielding; γ_{GEB} is the stress multiplier factor for global elastic buckling; and w_0 is the initial imperfection; $\frac{\gamma}{\gamma_{GEB}}$ is a utilization factor; and $\frac{1}{1-\frac{\gamma}{\gamma_{GEB}}}$ is an amplification factor.

The transformation process is questionable as it relies on the amplification factor that is based on $p - \delta$ effects of a beam under axial loads, which doesn't directly apply to a biaxially loaded orthotropic plate. While the assumption may hold for cases where longitudinal loads predominate, given that primary rigidity in a longitudinal stiffened panel comes from the stiffener, the response differs significantly in situations where the transverse loads predominate. Thus, employing the same amplification factor in such cases appears unreasonable.

In practice, transverse loads can induce a bending moment in the stiffener direction through magnified central displacements and thereby curvature change. The extent of displacement magnification under transverse loading is however much smaller than that of a beam analogy in which the major system rigidity comes from stiffeners in the longitudinal direction. In the absence of more accurate assessments of transverse loading contribution to the bending of longitudinal stiffeners, a practical way to modify the approach is to neglect this amplification factor for the contribution that comes from transverse loading.

This results in a modified bending moment formulation as:

$$M_0 = \left[F_x \frac{\gamma}{\gamma_{GEB} - \gamma} + (F_E - F_x) \frac{\gamma}{\gamma_{GEB}} \right] w_0 \tag{13}$$

where F_x is the applied longitudinal force to the stiffener. This applies for $F_E > F_x$, otherwise the elastic buckling of the stiffener is considered to occur.

If the loading scenario is transversely uniaxial, F_x approaches zero, giving a bending moment of $F_E \frac{\gamma}{\gamma_{GEB}} w_0$. It entails a bending moment where the lateral deformation of the stiffener directly scales with the global panel deformation. If the loading scenario is longitudinally uniaxial, F_x should approach F_E. The equation yields a bending moment of $F_E \frac{\gamma}{\gamma_{GEB} - \gamma} w_0$, which is the same as the original equation.

Fig. 22 shows the different failure categories with the modified IACS rule and the NLFEM results without the welding effects. In the L400 and L600 cases, the ultimate strength is determined by the local plate buckling limit when transverse stresses predominate. In the L1000 cases, it is plausible to consider the failure mode as global panel buckling when the loading scenario is nearly transversely uniaxial, as the ultimate strengths from both limits closely align. These modifications result in a notably improved agreement with numerical results for both the ultimate strength and the failure mode, as depicted in Figs. 22 and 19, compared to the outcomes obtained using the original rule.

When transverse stresses predominate, the stiffener yielding limit approaches the global panel buckling limit. This phenomenon arises from the denominator containing $\gamma_{GEB} - \gamma$ in equations. A precondition of $\gamma_{GEB} - \gamma > 0$ is valid, forcing that the stiffener yielding limit cannot be beyond the global panel buckling limit. The direct subtraction of stress multiplier factors implies an assumption of 'equivalent' loading processes and outcomes between the elastic buckling of a stiffener under axial loads (γ) and the elastic buckling of a plate under biaxial loads (γ_{GEB}). However, this assumption may be overly idealistic, particularly when longitudinal and transverse stresses are of similar magnitude. Under such conditions, interactions between biaxial loads are not adequately accounted for. Therefore, further research is imperative to enhance the accuracy of the approach in these scenarios.

- **Welding effects**

Welding effects include geometrical imperfections, residual stresses and material softening in HAZ. The IACS rule that was designed for steel panels, includes the effects of initial distortions, and the same shall apply to aluminium structures with carefully chosen

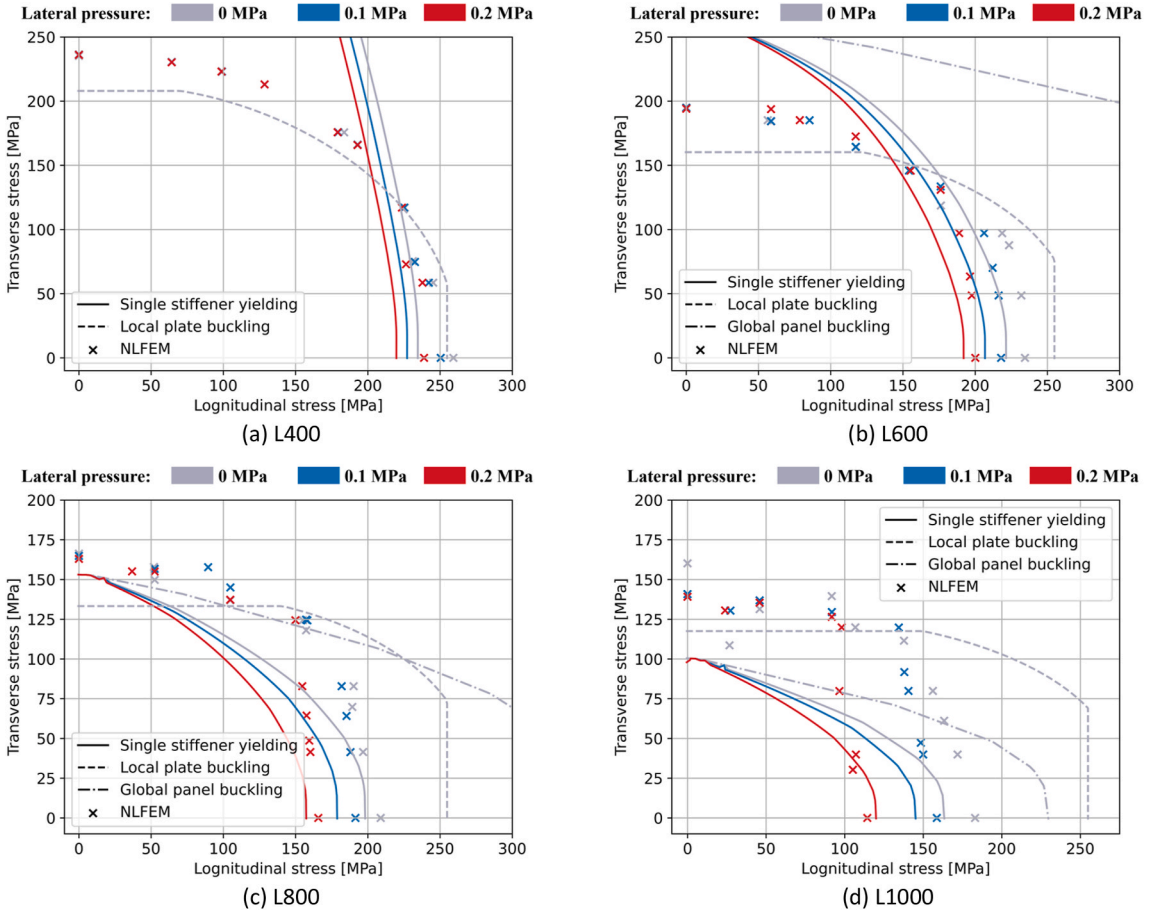

Fig. 22. Limit states with the modified IACS rule and NLFEM results under different lateral pressure levels.

amplitudes. Residual stresses are neglected in the IACS rule and this work, due to their generally small influence [20]. Material softening in HAZ substantially influences the ultimate strength and failure modes of aluminium structures, and is of major concern. The effects of material softening can be accounted for by reducing the allowable stress in the IACS rule to be the HAZ yield stress.

The following approach is proposed to include the welding effects of aluminium structures.

- In cases involving butt welding (extruded panels), the plate yield stress is adjusted to the HAZ yield stress for both local plate buckling and global panel buckling limits.
- In cases involving fillet welding (built-up panels), the evaluation point at the bottom of the stiffener adopts the HAZ yield stress as the specified minimum yield stress for the single stiffener yielding limit.

Ultimate limits with the proposed approach are shown in Fig. 23 together with the numerical results. The modification of transverse loads in Section 5.3 is also included. Only cases without the lateral pressure are included.

Generally, the modification gives reasonable predictions for welded aluminium panels. The influence of various welding patterns on the ultimate strength is effectively represented. As expected, lowering the plate yield stress (butt welding) in the local plate buckling limit and the global panel buckling limit diminishes both the longitudinal and transverse strength, while decreasing the yield stress at the stiffener bottom (fillet welding) primarily impairs the longitudinal stress limit. The reduction magnitude when longitudinal stresses predominate coincides with the NLFEM results also. Nevertheless, in the case of slender stiffened panels like L1000, the proposed approach leads to minimal change of the ultimate limit.

The study reveals that the method is sensitive to the slenderness of the panel. When considering butt welding effects across cases with varying panel lengths, the modification yields mean values of 0.87, 0.90, 0.94 and 0.85 between the rule predictions and the NLFEM results. When accounting for fillet welding effects, the modification produces mean values of 0.90, 0.89, 0.88 and 0.77.

It is observed that the ultimate limit is minimally influenced by the inclusion of welding effects in the case of slender panels, for both the modified IACS rule (Fig. 23-d) and the PULS approach (Fig. 18-b, -d and -e), despite the differing theoretical foundations of these two methods. This outcome is primarily attributed to criticality of the first yielding criterion at the stiffener's top in such cases, rendering changes in yield stresses at other locations inconsequential in determining the most conservative prediction.

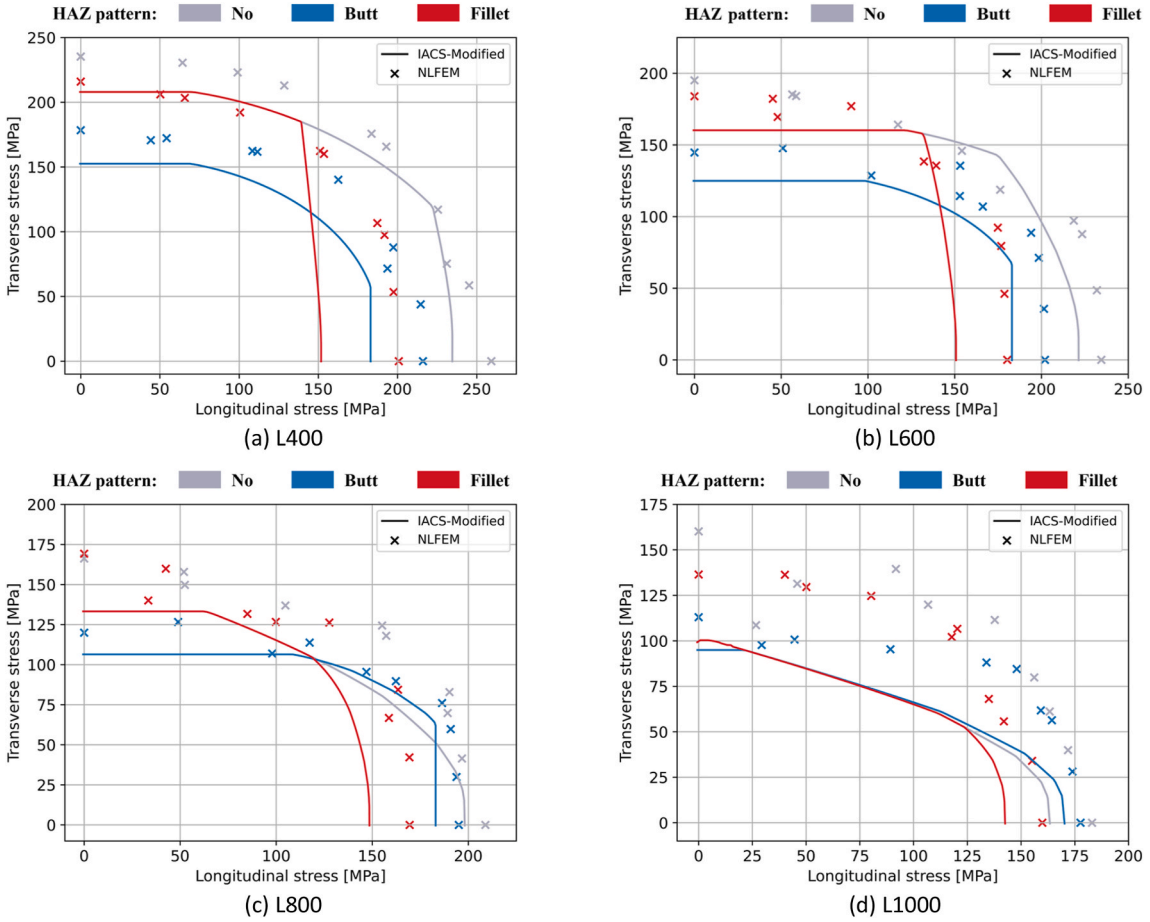

Fig. 23. Ultimate limit states of the modified approach in the modified IACS rule considering HAZ effects.

In summary, an adjustment of the yield stress within the IACS rule offers a reasonable means to predict the ultimate limit of welded aluminium stiffened panels. However, the effectiveness of this adjustment is influenced by the slenderness of the panels.

Notably, the slenderness ratio of aluminium structures consistently surpasses that of steel structures with similar geometries due to the smaller elastic modulus. This disparity poses a challenge when attempting to apply existing design rules developed for steel structures to aluminium structures. For example, in the IACS Common Structural Rule S35 Buckling Strength Assessment of Ship Structure Elements [54], that will come into force in July 2024, one global deformation reduction factor is introduced. The factor is empirical and depends upon the global slenderness ratio. These values may not be directly applicable to aluminium structures. Hence, further research and necessary modifications are imperative to provide a deeper understanding and to enhance the accuracy of predictions.

5.4. Potential limitations

The current study contains various assumptions that are introduced in the numerical simulations and hence influence the proposed modification of the design method. The limitations of the study and their implications for future work are summarized as follows.

- In the numerical simulations, the modelling of HAZ effects is mainly calibrated to previous experiments. It is acknowledged that the material curves, the HAZ width, the reduction factor of softening, the difference between butt- and fillet-welding contents are highly dependent on material compositions, structural geometries, and welding parameters. The current work focuses on traditional welding technique such as metal inert gas (MIG) and Tungsten inert gas (TIG) welding. Special welding techniques, such friction stir welding (FSW), may have a big impact on these assumptions. Parametric studies are suggested to better understand how potentially changed factors may influence the observations and conclusions obtained in this work.
- In the proposed modified design method, a linear reduction of the axial loads is assumed to account for the effects of transverse load. This is simple first approach, but more investigation is needed to reveal the physics of the load interaction. A more precise method should be developed in the future.

- When considering welding effects, material softening factor plays an important role. Reduction factors may be calibrated to experimental results, as done in this work, but is generally limited to open access publications. Alternatively, factors given in design rules for aluminium civil structures, such as Eurocode 9 [58], could be adopted, but their validity should also be verified by comparison with numerical simulations or experiments.

6. Conclusions

Numerical simulations of welded aluminium stiffened panels subjected to biaxial compression and lateral pressure were conducted. Ultimate strength and failure modes with different panel length, welding patterns and combined loads were studied. Ultimate limits predicted by two design methods were compared with ultimate strength from the simulations. Limitations of the design methods were discussed when they are used for welded aluminium stiffened panels. Potential modifications of the IACS rule were suggested to be applied for aluminium structures. The main conclusions are summarized as follows.

- Failure modes of aluminium stiffened panels depend on the load combinations, dimensions and welding patterns, thus affecting ultimate strength. Collapse induced by beam-column buckling of stiffeners normally happens with predominant longitudinal stresses. In this case, fillet welding deteriorates the stiffener capacity substantially, and butt welding also affects the panel strength by reducing the attached plate capacity. Collapse induced by local plate buckling happens with predominant transverse stresses. Butt welding reduces ultimate strength significantly while fillet welding influences little in this case.
- When welding effects are not included, both the IACS rule and the PULS approach can give good ultimate limit predictions. The predictions from the IACS rule are more conservative than those from the PULS approach. Both methods show decreasing conservatism compared to the numerical results with increasing lateral pressure. When welding effects are included in the PULS approach, the butt welding cases (extruded profiles) have a better agreement to the numerical results than the fillet welding cases (built-up profiles).
- The IACS rule exhibits overly conservative predictions of the ultimate strength when transverse stresses dominate. This may be due to the improper consideration of the $p-\delta$ effects for transverse loading in the calculation of stiffener bending moment at midspan. Potential corrections are recommended by removing the amplification factor for transverse loading. The modified formulation produces higher predictions and aligns better with numerical simulations. Further investigation is essential to comprehensively understand the equivalence between the assumed load scenarios and to incorporate interactions between biaxial loads more accurately.
- The IACS rule has a potential to be adopted for aluminium structures. To achieve that, the lateral pressure effects should be modified to reflect the sensitivity of aluminium structures to the global panel failure mode. The effects are not included in both the local plate and global panel evaluation in the current rule. A complete consideration of the effects could improve the accuracy of the global stiffened panel limit and keep constant conservative predictions of the single stiffener yielding limit. It is also noticed that the PULS approach shows a less accurate ultimate limit predictions for increasing larger lateral pressure level.
- To account for welding effects on aluminium stiffened panels within the framework of the IACS rule, it is proposed to adjust the yield stress in different limits for various welding configurations. In case of butt-welded panels, the plate yield stress is reduced for both local plate buckling and global panel buckling limits. In case of fillet-welded panels, the bottom of the stiffener should adopt the HAZ yield stress for the single stiffener yielding limit. The proposed approach effectively addresses the influence of welding effects on the ultimate strength, yet its performance depends on the slenderness of the panel. Therefore, additional investigation and refinements are needed to further enhance accuracy and robustness in these predictions.

CRediT authorship contribution statement

Xintong Wang: Writing – review & editing, Writing – original draft, Visualization, Methodology, Conceptualization. **Zhaolong Yu:** Writing – review & editing, Supervision, Methodology. **Jørgen Amdahl:** Writing – review & editing, Supervision, Methodology.

Declaration of competing interest

The authors declare that they have no known competing financial interests or personal relationships that could have appeared to influence the work reported in this paper.

Data availability

Data will be made available on request.

Acknowledgements

The authors gratefully acknowledge the support from the Research Council of Norway under the Knowledge-Building Project for Industry Robot Welding of Aluminium Ship Hulls [grant number: KPN295138]. Part of this work is also supported by the Centre for Autonomous Marine Operations and Systems (AMOS) [project number: 223254]. The authors would also like to thank the support from high performance computation resources from the Norwegian national e-infrastructures, Project NN9585K - Accidental actions

on strait crossings and offshore platforms.

References

[1] Hosseinabadi OF, Khedmati MR. A review on ultimate strength of aluminium structural elements and systems for marine applications. Ocean Eng 2021;232:109153.
[2] Shanmugam NE, Dongqi Z, Choo YS, Arockiaswamy M. Experimental studies on stiffened plates under in-plane load and lateral pressure. Thin-Walled Struct 2014;80:22–31.
[3] Cui J, Wang D. An experimental and numerical investigation on ultimate strength of stiffened plates with opening and perforation corrosion. Ocean Eng 2020;205:107282.
[4] Liu B, Gao L, Ao L, Wu W. Experimental and numerical analysis of ultimate compressive strength of stiffened panel with openings. Ocean Eng 2021;220:108453.
[5] Ma H, Xiong Q, Wang D. Experimental and numerical study on the ultimate strength of stiffened plates subjected to combined biaxial compression and lateral loads. Ocean Eng 2021;228:108928.
[6] Benson S, Downes J, Dow RS. Compartment level progressive collapse analysis of lightweight ship structures. Mar Struct 2013;31:44–62.
[7] Benson S, Downes J, Dow RS. Overall buckling of lightweight stiffened panels using an adapted orthotropic plate method. Eng Struct 2015;85:107–17.
[8] Khedmati MR, Zareei MR, Rigo P. Sensitivity analysis on the elastic buckling and ultimate strength of continuous stiffened aluminium plates under combined in-plane compression and lateral pressure. Thin-Walled Struct 2009;47:1232–45.
[9] Khedmati MR, Bayatfar A, Rigo P. Post-buckling behaviour and strength of multi-stiffened aluminium panels under combined axial compression and lateral pressure. Mar Struct 2010;23:39–66.
[10] Khedmati MR, Pedram M, Rigo P. The effects of geometrical imperfections on the ultimate strength of aluminium stiffened plates subject to combined uniaxial compression and lateral pressure. Ships Offshore Struct 2014;9:88–109.
[11] Khedmati MR, Memarian HR, Fadavie M, Zareei MR. Empirical formulations for estimation of ultimate strength of continuous aluminium stiffened plates under combined transverse compression and lateral pressure. Ships Offshore Struct 2016;11:258–77.
[12] Khedmati MR, Memarian HR, Fadavie M, Zareei MR. Ultimate strength of continuous stiffened aluminium plates under combined biaxial compression and lateral pressure. Lat Am J Solid Struct 2015;12:1698–720.
[13] Rigo P, Sarghiuta R, Estefen S, Lehmann E, Otelea SC, Pasqualino I, et al. Sensitivity analysis on ultimate strength of aluminium stiffened panels. Mar Struct 2003;16:437–68.
[14] Ringsberg JW, Darie I, Nahshon K, Shilling G, Vaz MA, Benson S, et al. The ISSC 2022 committee III.1-Ultimate strength benchmark study on the ultimate limit state analysis of a stiffened plate structure subjected to uniaxial compressive loads. Mar Struct 2021;79:103026.
[15] Yao T, Fujikubo M. Buckling and ultimate strength of ship and ship-like floating structures. Butterworth-Heinemann; 2016.
[16] Wang, X, & Amdahl, J. "Analysis of Welding Influences on Extruded Aluminum Panel Buckling." Proceedings of the ASME 2022 41st International Conference on Ocean, Offshore and Arctic Engineering. Volume 2: Structures, Safety, and Reliability. Hamburg, Germany. June 5–10, 2022. V002T02A073. ASME. https://doi.org/10.1115/OMAE2022-78575.
[17] Paik JK, Andrieu C, Cojeen HP. Mechanical collapse testing on aluminum stiffened plate structures for marine applications. Mar Technol 2008;45:228.
[18] Georgiadis DG, Samuelides MS. Stochastic geometric imperfections of plate elements and their impact on the probabilistic ultimate strength assessment of plates and hull-girders. Mar Struct 2021;76:102920.
[19] Georgiadis D, Samuelides M, Li S, Kim D, Benson S. Influence of stochastic geometric imperfection on the ultimate strength of stiffened panel in compression. In: Developments in the analysis and design of marine structures: CRC Press; 2021. p. 95–103.
[20] Wang X, Amdahl J, Egeland O. Numerical study on buckling of aluminum extruded panels considering welding effects. Mar Struct 2022;84:103230.
[21] Li S, Kim DK, Benson S. The influence of residual stress on the ultimate strength of longitudinally compressed stiffened panels. Ocean Eng 2021;231:108839.
[22] Zha Y, Moan T. Ultimate strength of stiffened aluminium panels with predominantly torsional failure modes. Thin-Walled Struct 2001;39:631–48.
[23] Hopperstad OS, Langseth M, Hanssen L. Ultimate compressive strength of plate elements in aluminium: correlation of finite element analyses and tests. Thin-Walled Struct 1997;29:31–46.
[24] Benson S, Downes J, Dow RS. Ultimate strength characteristics of aluminium plates for high-speed vessels. Ships Offshore Struct 2011;6:67–80.
[25] Magoga T, Flockhart C. Effect of weld-induced imperfections on the ultimate strength of an aluminium patrol boat determined by the ISFEM rapid assessment method. Ships Offshore Struct 2014;9:218–35.
[26] Zha Y, Moan T. Experimental and numerical prediction of collapse of flatbar stiffeners in aluminum panels. J Struct Eng 2003;129:160–8.
[27] Paik JK. Buckling collapse testing of friction stir welded aluminum stiffened plate structures. Report SR-1454 Washington (DC): Ship Structure Committee 2009.
[28] Kee Paik J, Ju Kim B, Min Sohn J, Hoon Kim S, Min Jeong J, Seok Park J. On buckling collapse of a fusion-welded aluminum-stiffened plate structure: an experimental and numerical study. J Offshore Mech Arctic Eng 2011;134.
[29] Paulo RMF, Teixeira-Dias F, Valente RAF. Numerical simulation of aluminium stiffened panels subjected to axial compression: sensitivity analyses to initial geometrical imperfections and material properties. Thin-Walled Struct 2013;62:65–74.
[30] Farajkhah V, Liu Y. Effect of fabrication methods on the ultimate strength of aluminum hull girders. Ocean Eng 2016;114:269–79.
[31] Paulo RMF, Rubino F, Valente RAF, Teixeira-Dias F, Carlone P. Modelling of friction stir welding and its influence on the structural behaviour of aluminium stiffened panels. Thin-Walled Struct 2020;157:107128.
[32] Guo Z, Bai R, Lei Z, Jiang H, Zou J, Yan C. Experimental and numerical investigation on ultimate strength of laser-welded stiffened plates considering welding deformation and residual stresses. Ocean Eng 2021;234:109239.
[33] Brubak L, Bøe A, Lv Y, Ishibashi K, Bollero A. Rule formulation updates on buckling strength requirements in Common Structural Rules. In: Advances in the analysis and design of marine structures. CRC Press; 2023. p. 339–46.
[34] Societies IAoC. Common structural rules for bulk carriers and oil tankers. London, UK: CSR); 2018.
[35] Class guideline DNV. DNV-CG-0128 Buckling. Class guideline-Buckling. 2021. Edition October.
[36] DnV RC201. Structural design of offshore units (WSD method). 2004.
[37] Solland G, Jensen PlG. Background to DNV recommended practice DNV-RP-C201 buckling strength of plated structures. 2004. p. 979–86.
[38] Byklum E. Ultimate strength analysis of stiffened steel and aluminium panels using semi-analytical methods: fakultet for ingeniørvitenskap og teknologi. 2002.
[39] Byklum E, Amdahl J. A simplified method for elastic large deflection analysis of plates and stiffened panels due to local buckling. Thin-Walled Struct 2002;40:925–53.
[40] Byklum E, Steen E, Amdahl J. A semi-analytical model for global buckling and postbuckling analysis of stiffened panels. Thin-Walled Struct 2004;42:701–17.
[41] Veritas DN. User manual nauticus hull - PULS. Norway: Høvik; 2015.
[42] Paik JK, Thayamballi AK, Ju Kim B. Large deflection orthotropic plate approach to develop ultimate strength formulations for stiffened panels under combined biaxial compression/tension and lateral pressure. Thin-Walled Struct 2001;39:215–46.
[43] Paik JK, Thayamballi AK, Lee SK, Kang SJ. A semi-analytical method for the elastic-plastic large deflection analysis of welded steel or aluminum plating under combined in-plane and lateral pressure loads. Thin-Walled Struct 2001;39:125–52.
[44] Paik JK, Lee MS. A semi-analytical method for the elastic–plastic large deflection analysis of stiffened panels under combined biaxial compression/tension, biaxial in-plane bending, edge shear, and lateral pressure loads. Thin-Walled Struct 2005;43:375–410.
[45] Wang, X, & Amdahl, J. "How Loads Interact? A Numerical Investigation of Aluminum Stiffened Panels Under Bi-Axial and Lateral Loads." Proceedings of the ASME 2023 42nd International Conference on Ocean, Offshore and Arctic Engineering. Volume 2: Structures, Safety, and Reliability. Melbourne, Australia. June 11–16, 2023. V002T02A054. ASME. https://doi.org/10.1115/OMAE2023-100743.

[46] Marketing ZM. 60 m jumbo-cat from fjellstrand AS. https://boatdiesel.com/News/ZF-Marine/N-109/60-m-Jumbo-Cat-from-Fjellstrand-AS.cfm. [Accessed 10 April 2024].
[47] DNV. Rules for classification: high speed and light craft (RU-HSLC). Norway: DNV AS; 2023.
[48] Steen E, Byklum E, Hellesland J. Elastic postbuckling stiffness of biaxially compressed rectangular plates. Eng Struct 2008;30:2631–43.
[49] Paik JK, Seo JK. Nonlinear finite element method models for ultimate strength analysis of steel stiffened-plate structures under combined biaxial compression and lateral pressure actions—Part I: plate elements. Thin-Walled Struct 2009;47:1008–17.
[50] Paik JK, Seo JK. Nonlinear finite element method models for ultimate strength analysis of steel stiffened-plate structures under combined biaxial compression and lateral pressure actions—Part II: stiffened panels. Thin-Walled Struct 2009;47:998–1007.
[51] Li D, Chen Z. Advanced empirical formulae for the ultimate strength assessment of continuous hull plate under combined biaxial compression and lateral pressure. Eng Struct 2023;285:116041.
[52] Manual AU. Abaqus user manual. Abaqus; 2020.
[53] Aalberg A, Langseth M, Larsen PK. Stiffened aluminium panels subjected to axial compression. Thin-Walled Struct 2001;39:861–85.
[54] Hydro. Technical datasheet - extruded products alloy EN AW-6082 [AlSi1MgMn]. 2019.
[55] Offshore Standards DNV. DNV-OS-C401 fabrication and testing of offshore structures. July. 2023.
[56] Rønning L, Aalberg A, Kristian Larsen P. An experimental study of ultimate compressive strength of transversely stiffened aluminium panels. Thin-Walled Struct 2010;48:357–72.
[57] Ahn J, He E, Chen L, Wimpory RC, Kabra S, Dear JP, et al. FEM prediction of welding residual stresses in fibre laser-welded AA 2024-T3 and comparison with experimental measurement. Int J Adv Des Manuf Technol 2018;95:4243–63.